metals

MDPI

Article

The Hot Ductility, Microstructures, Mechanical Properties and Corrosion Resistance in an Advanced Boron-Containing Complex Phase Steel Heat-Treated Using the Quenching and Partitioning (Q&P) Process

Antonio Enrique Salas-Reyes [1,*], Gerardo Altamirano-Guerrero [2], Rogelio Deaquino [3], Armando Salinas [3], Gabriel Lara-Rodriguez [4], Ignacio Alejandro Figueroa [4], Jesús Rafael González-Parra [1,5] and Barrie Mintz [6]

[1] Departamento de Ingeniería Metalúrgica, Facultad de Química, UNAM, Ciudad de México 04510, Mexico
[2] División de Estudios de Posgrado e Investigación, Tecnológico Nacional de México/IT de Saltillo, Coahuila 25280, Mexico
[3] Centro de Investigación y de Estudios Avanzados del Instituto Politécnico Nacional, Unidad Saltillo, Coahuila 25900, Mexico
[4] Instituto de Investigaciones en Materiales, UNAM, Ciudad de México 04510, Mexico
[5] Centro de Ingeniería de Superficies y Acabados, Facultad de Ingeniería, UNAM, Ciudad de México 04510, Mexico
[6] Department of Mechanical Engineering and Aeronautics, City University of London, London EC1V 0HB, UK
* Correspondence: enriquesalas@comunidad.unam.mx; Tel.: +52-55-5622-5243

Abstract: The objective of this research work is to obtain the hot ductility behavior, and the structural, microstructural and mechanical characteristics of one of the latest generation of AHSS steels, a complex phase (CP) steel microalloyed with boron (0.006 wt.%), processed by hot and cold rolling operations and heat-treated using two different quenching and partitioning (Q&P) treatments, a one-step partitioning (quenching to 420 °C) and the other a two-step partitioning (quenching to 420 °C and reheated to 600 °C). The results show that boron has a marked effect on the solidification process of the CP steel, refining the austenitic grain size. Due to its refinement, the boron-containing steel had better ductility throughout the temperature range examined (700–900 °C), i.e., the hot ductility trough. Thus, the minimum percentage of reduction in area (%RA) value occurring at 800 °C was 43% for the boron-free steel, compared with 58% for the boron-containing steel. Hence, cracking would not be a problem when straightening the strand on continuous casting. The benefit of boron addition on the room temperature properties was found to be very marked for the higher temperature two-step partitioning treatment, giving a yield stress of 1200 MPa, a UTS (ultimate tensile strength) of 1590 MPa and a total elongation above 11%. The final Q&P microstructure, in both one- and two-step partitioning conditions, consisted of retained austenite (RA-γ), martensite and ferrite islands in a bainitic matrix. Furthermore, the boron treated steel on quenching produced a greater amount of RA-γ, which accounted for its better room temperature ductility and produced a martensitic matrix rather than a bainitic one, giving it greater strength. The addition of boron improved the corrosion resistance of this type of third generation AHSS steel.

Keywords: hot ductility behavior; complex phase steel; quenching and partitioning (Q&P) steel; boron content; multiphasic microstructure; mechanical properties; corrosion resistance

Citation: Salas-Reyes, A.E.; Altamirano-Guerrero, G.; Deaquino, R.; Salinas, A.; Lara-Rodriguez, G.; Figueroa, I.A.; González-Parra, J.R.; Mintz, B. The Hot Ductility, Microstructures, Mechanical Properties and Corrosion Resistance in an Advanced Boron-Containing Complex Phase Steel Heat-Treated Using the Quenching and Partitioning (Q&P) Process. *Metals* **2023**, *13*, 257. https://doi.org/10.3390/met13020257

Academic Editor: Andrey Belyakov

Received: 11 December 2022
Revised: 16 January 2023
Accepted: 20 January 2023
Published: 28 January 2023

1. Introduction

Steel is the most recycled material in the world, and almost all of the advanced high strength steel (AHSS) grades can be made from 100% steel scrap by employing an electric arc furnace (EAF). In addition, the production route using scrap in an EAF allows secondary steelmaking, two technologies that are powered principally by electricity coming from renewable energy.

However, recycled steel scrap generally has a complex chemical nature (i.e., mixing of different quality types of scrap). This mixing can represent a serious problem during the continuous casting (CC) of molten steel due to the presence of impurities and/or residual elements. Impurities and/or residuals elements are very difficult to refine from molten metal under the governing metallurgical thermodynamics and kinetics. Additionally, highly-alloyed or microalloyed steel grades, usually termed as special steels, are difficult to cast using the CC technology. Cracks are prone to form on the surface of semi-products during the straightening operation of strands. These cracks form in the temperature range of 700–1000 °C, the same temperature range in which ductility is poor, as measured by the percentage reduction in transversal area (%RA) in a hot tensile test. This range corresponds to when on cooling, a thin film of ferrite can form surrounding the prior austenite grain boundaries. The ferrite being softer than the austenite allows the strain to concentrate there, causing intergranular failure. This can occur for a wide variety of steel grades [1].

As well as the addition of boron (B) often improving the hot ductility, it can also lead to difficulties during steel casting due to the presence of dissolved nitrogen in the molten steel forming harmful boron nitride (BN) compounds. During the last ten years, several efforts have been reported that explain the influence of B content on the hot ductility behavior of microalloyed steels [2–5] and advanced high strength steels (AHSS), including low-carbon advanced ultra-high strength steels [6] and TWIP steels [7–10]. Mintz and Crowther [1] reviewed boron's relationship with other microalloying elements (i.e., Ti and Nb) on the hot ductility behavior of these steels and concluded that if boron nitride is allowed to form, ductility can be poor, but if boron is allowed to segregate uninterruptedly to the boundaries, it can strengthen them and improve the hot ductility. Thus, the cooling rate is found to be important, and Ti is often added as a N getter to protect the steel from forming BN.

Today AHSS are constantly evolving with increasing strength, ductility, rigidity, hardness and toughness to satisfy increasing engineering demands. It is evident that the high-mechanical performance behavior of AHSS depends strongly on the selection of chemical composition and sophisticated technologies for applying well-controlled thermo-mechanical, mechanical and thermal treatments. A well-designed metallurgical pathway must include a complete steel processing route from the initial stage of casting to the last operation during its mechanical forming, and to accomplish this, the automotive and steelmaking industries are working together in further developing AHSS.

The use of AHSS in vehicles offers substantial weight reduction possibilities (e.g., 25–40% in a vehicle's mass) compared with conventional carbon steels. This is one of the main reasons steelmakers are interested in fabricating AHSS. The diversity of microstructures in these steels is obtained through compositional and thermo-mechanical control process (TMCP) and careful heat treatments [11].

The new class of third-generation AHSS, which includes quenching and partitioning (Q&P) steels, can achieve these complex phase microstructures and is emerging in the automotive industry as a new type of ferrous alloy with potentially outstanding mechanical properties. These positive properties are due to the formation of retained austenite, which is enriched with C on partitioning, resulting in its stabilization, and the presence of martensite, which increases the strength and also can supply C to the austenite. Speer et al. [12,13] have been very active in developing the microstructures required in these Q&P steels and the partitioning step pathways obtained by a thermal processing route. This includes a quenching step carried out between the martensite-start (Ms) and martensite-finish (M_f) temperatures, which is then followed by a partitioning step carried out in one-step (quenching to the partitioning temperature) or two steps (quenching to the partitioning temperature and then reheating to a higher temperature). Thus, partitioning allows carbon enrichment of the austenite not only from a bainitic matrix but also from supersaturated martensite.

Initially, it was thought that the quenching operation had to be carried out strictly between the M_s and M_f to promote the microstructural conditions that result in the best mechanical properties after partitioning. However, it has been proved that advanced multi-

phasic high strength steels can be heat-treated by the Q&P method even when quenching above the M_s temperature (i.e., above or below in the limits of the M_s transformation line). On this basis, Li et al. [14] proposed a new steel processing strategy. This thermal processing combines dynamic carbon partitioning during an easily controlled processing route for hot-rolled steel. A similar method focused on lower temperature austenite decomposition was proposed by Pashangeh et al. [15], which depends on the control of the partial transformation of bainite (quenching and bainitic holding (Q&B) above the M_s temperature). Thus, a multiphasic microstructure can be achieved that consists of a hard bainite/martensite mixture, soft islands of RA-γ, well-distributed ferrite and some carbide precipitation and that has superior mechanical resistance and ductility. In Q&P steels, these types of mixtures of phases and constituents have shown higher corrosion resistance in NaCl solutions due to the decrease in the residual tensile stresses on the Q&P steel surface through using a higher temperature in the second stage, and consequently, the insidious localized pitting does not occur [16].

Considering the above concepts, this research work investigates the effect of boron content on the relationship between hot ductility and post microstructural conditioning. The investigation is performed on an experimental highly-alloyed low carbon boron-containing complex phase (CP) steel fabricated following the Q&P thermal concept route. The relationship between room temperature mechanical resistance and corrosion is also investigated with particular attention being given to the effects of the boron content.

Thus, the present paper attempts to assess the effects of boron on the various stages of the processing route for the manufacture of Q&P steels from casting to the partitioning operation heat treatment.

2. Materials and Methods

An experimental advanced complex phase (CP) steel was fabricated by induction melting. Melting was carried out under open-air conditions employing steel scrap of known composition and ferroalloys so as to follow the normal EAF (electric arc furnace) processing route. Subsequently, molten steel was poured into 15 kg capacity single preheated ladles, one of which was B-free and the other one had a boron microaddition. The castings were carried out in sand molds 6.5 cm × 6.5 cm × 24 cm in dimension, and the resulting steel ingots were identified as CP-B0 (the boron-free steel of reference) and CP-B60 (the boron-containing steel). Table 1 lists the chemical composition of both CP steels, as determined by spark atomic emission spectroscopy (Spectro M11 spectrometer, Spectro Scientific by AMETEK Inc., Mahwah, NJ, USA) and elemental combustion spectroscopy (CS-200 LECO spectrometer, LECO Instruments Ltd., Stockport, UK). The base composition of the steel was 0.15% C, 2% Mn, and 0.6% Si with "residual" levels of Cr, Ni, Mo and Cu. An addition of Ti (0.015%) and a high Nb addition of 0.15% were made to the steels. The two steels had essentially the same composition except steel CP-B60 had a 0.0060% B addition.

The volume fraction and temperature at which the important second phases precipitated out at, during and after steel solidification, were calculated using JMatPro software (Java-based Materials Properties, 9.0 version, Sente Software Ltd., Guildford, UK). For this, the general steel database was employed, running calculations from 1600 °C to room temperature every 10 °C. The theoretical time–temperature transformation (TTT) diagrams for both CP steels were also estimated as a function of grain size and intercritical temperatures during cooling.

After casting, the CP-B0 and CP-B60 steel ingots were cut to obtain samples for metallographic analysis in the as-cast condition. For the solidification microstructure observation, a location close to the bottom part of the ingots was chosen and a metallographic examination was carried out using the conventional procedure. The chemical solution used for revealing the solidification microstructure was composed of 0.5 g of $CuCl_2$, 0.5 g of $FeCl_3$, 30 mL of H_2O, 10 mL of HCl and 8 mL of C_2H_6O. The samples were etched by immersion for 50 s at room temperature. The solidification microstructure was analyzed at different magnifications using an Olympus PMG 3 optical microscope (Olympus Scientific

Solutions Technologies Incorporated, Waltham, MA, USA). Representative microstructures were used for the measurement of the austenitic grain size through SigmaScan Pro image analyzer software (5.0, Systat Software Inc., San Jose, CA, USA). The solidification structures of both steels were characterized employing the scanning electron microscopy-electron backscatter diffraction (SEM-EBSD) technique. For this, samples with dimensions of 0.25 cm × 1.0 cm × 1.0 cm were surface prepared using colloidal silica solution and polishing for 6 h to ensure Kikuchi diffraction indexing patterns. Then, the samples were pasted on SEM holders and painted with silver. The EBSD scans were carried out at a SEM magnification of 20× using 7 μm as a step size. Post-processing of the SEM-EBSD data was carried out using Channel 5 system software (Oxford Instruments HKL A/S, Oxofordshire, UK). Finally, in order to identify the phases present in the as-cast condition, X-ray diffraction measurements were performed in a Siemens D5000 diffractometer (Siemens AG, Munich, Germany) using Co Kα electromagnetic radiation (45 kV-18 mA) with a diffractomer angle 2θ from 20 to 120°. A scanning step of 0.013° and a counting time of 13.7 s were used.

Table 1. Chemical composition of the experimental advanced high strength complex phase (CP) steels (in wt.%).

Element	CP-B0 Steel	CP-B60 Steel
C	0.16	0.16
Mn	1.94	1.93
Si	0.591	0.59
Cr	0.44	0.44
Ni	0.12	0.12
Mo	0.401	0.397
Cu	0.068	0.068
Nb	0.151	0.156
Ti	0.018	0.014
V	0.01	0.01
Al	0.012	0.01
S	0.031	0.03
P	0.022	0.023
N	0.012	0.012
B	0	0.006
Fe	Bal.	Bal.

In the same solidification condition, cylindrical tensile specimens of 6 mm diameter and 36 mm gauge length were machined to evaluate the hot ductility of both the boron-free (CP-B0) and boron-containing (CP-B60) steels. Isothermal uniaxial hot tensile tests were annealed at 1100 °C and tensile tested at 700, 750, 800, 850 and 900 °C, the temperature range in which it is expected that a loss of ductility occurs (i.e., the trough where the ductility can be very poor). The specimens were strained to failure at a constant strain rate of 1×10^{-3} s^{-1}. For this purpose, a servo hydraulic universal testing machine equipped with a radiant cylindrical furnace, also instrumented with K-type probe thermocouple sensors, was employed. The applied thermal cycle consisted of heating from room temperature to a target temperature of 1100 °C at a rate of 75 °C/min. Once this temperature was reached, the samples were soaked for 15 min. Then, each tensile specimen was cooled down as quickly as possible using argon flow to the target temperature and maintained there for 5 min before straining. Argon again served as a protective gas in the furnace chamber inhibiting the steel oxidizing during hot testing, and was maintained at a constant flow rate throughout the testing. After fracture, the strained specimens were cooled down to room temperature using the argon gas as a quenching media. SEM fracture surface images of strained specimens were then digitally treated to measure the reduction in transverse area (% of RA) and these values were used to plot the hot ductility curves. As an effort to correlate the hot ductility behavior of steels with the transforming microstructure (i.e.,

$\gamma \rightarrow \gamma + \alpha \rightarrow \alpha$) during straining, the Ar_1, Ar_3 and Ae_3 intercritical temperatures and the M_s and M_f transformation temperatures for each steel were determined by dilatometric testing in a Linseis L78-RITA quenching dilatometer (Linseis Inc., Robbinsville, NJ, USA). These tests were carried out on samples with dimensions of 50 mm$\times$ 11 mm $\times$ 1.2 mm and were heated at a constant heating rate of 20 °C/s from room temperature to 1100 °C, homogenized for 10 min and quenched at a cooling rate of 200 °C/s by helium gas to room temperature.

For the subsequent steel processing (i.e., thermo-mechanical, mechanical and thermal cycling operations), samples of 5 cm length, 2.5 cm width and 2.5 cm in thickness were cut from each steel ingot. The samples were protected from oxidation by a film of zirconium oxide coating and then heated from room temperature at a constant rate of 300 °C/h to 1250 °C and homogenized for 3.5 h. Immediately, they were hot-rolled by applying eight passes at a constant feeding rate of 15 mpm (meter per minute). The finishing rolling thickness was 5 mm, resulting in a total reduction equal to 80%. After this, and as an attempt to conserve the metallurgical products of the thermo-mechanical processing, each hot-rolled steel sample was rapidly cooled from approximately 800 °C to room temperature by quenching each strip in oil. After this, the strips were immediately cold-rolled at a constant feeding rate of 20 mpm until a final thickness of 1 mm was achieved. For these rolling schedules, a reversible 25 HP power Fenn Amca rolling mill (International Rolling Mills, Pawtucket, RI, USA) was employed.

The cold-rolled steel sheets were subjected to the quenching and partitioning (Q&P) heat treatment for both the one-step (P1) and two-step (P2) partitioning step pathways (see Figure 1). The employed thermal cycle for the one-step partitioning (P1) route consisted of reheating from room temperature to 1100 °C, holding for 15 min, followed by quenching in a salt bath set at 420 °C and isothermal holding for 8 min to allow partitioning to occur and, finally, fast cooling in oil to room temperature. The second employed thermal cycle for the two-step partitioning (P2) route consisted of same conditions as for the P1 route, but after quenching in the salt bath, the partition operation was carried out in a furnace set at 600 °C. A holding time of 6.5 min was applied, followed by fast cooling in oil to room temperature. It is important to mention that after the quenching into the salt bath, every sample was subjected to vigorous manual stirring for 30 s and held another 60 s (soaking stage) to unify the temperature in the samples and ensure the breaking down of the thermal steam film around the sample surface. This operation was performed for both the P1 and P2 partitioning step pathways. Thus, samples for the Q&P thermal cycles were identified as CP-B0-Q&P-P1, CP-B0-Q&P-P2 for the boron-free steel given the P1 and P2 partitioning treatment and as CP-B60-Q&P-P1, CP-B60-Q&P-P2, for the boron-treated steel. The quenching temperature was set at 420 °C for all the studied cases. This quenching temperature signifies a cooling condition above the M_s temperature transformation (310 °C), where partial bainitic transformation is present. Figure 1 illustrates the complete microstructure conditioning for the studied CP steel.

To determine the phases formed after the Q&P treatments, X-ray diffraction tests were carried out in a Brucker D8 Advance Eco Diffractometer (Bruker Corporation, Billerica, MA, USA) from 20° to 120° in 2θ and with a step size of 0.02°, employing a Cu filament.

For the SEM examinations, a standard metallographic sample preparation was used as described above for the optical microscope examinations. However, a final polishing step was carried out using the same colloidal silica solution for 5 h. This sample preparation technique can help to reveal the microstructural features of the heat-treated steels more readily. It should be noted that the samples were cleaned with distilled water, ethyl alcohol and hot air. As a final step before SEM examination, for a more effective cleaning, which eliminates particles of the abrasive agent, an ultrasonic bath was used for 15 min, followed by drying with hot air. The microstructure of Q&P steels was revealed by immersion for 35 s at 70 °C using a modified composition of LePera reactant. The microstructural characterization of the Q&P steels was carried out at different magnifications using a JEOL JMS-7800 F (JEOL Ltd., Tokio, Japan).

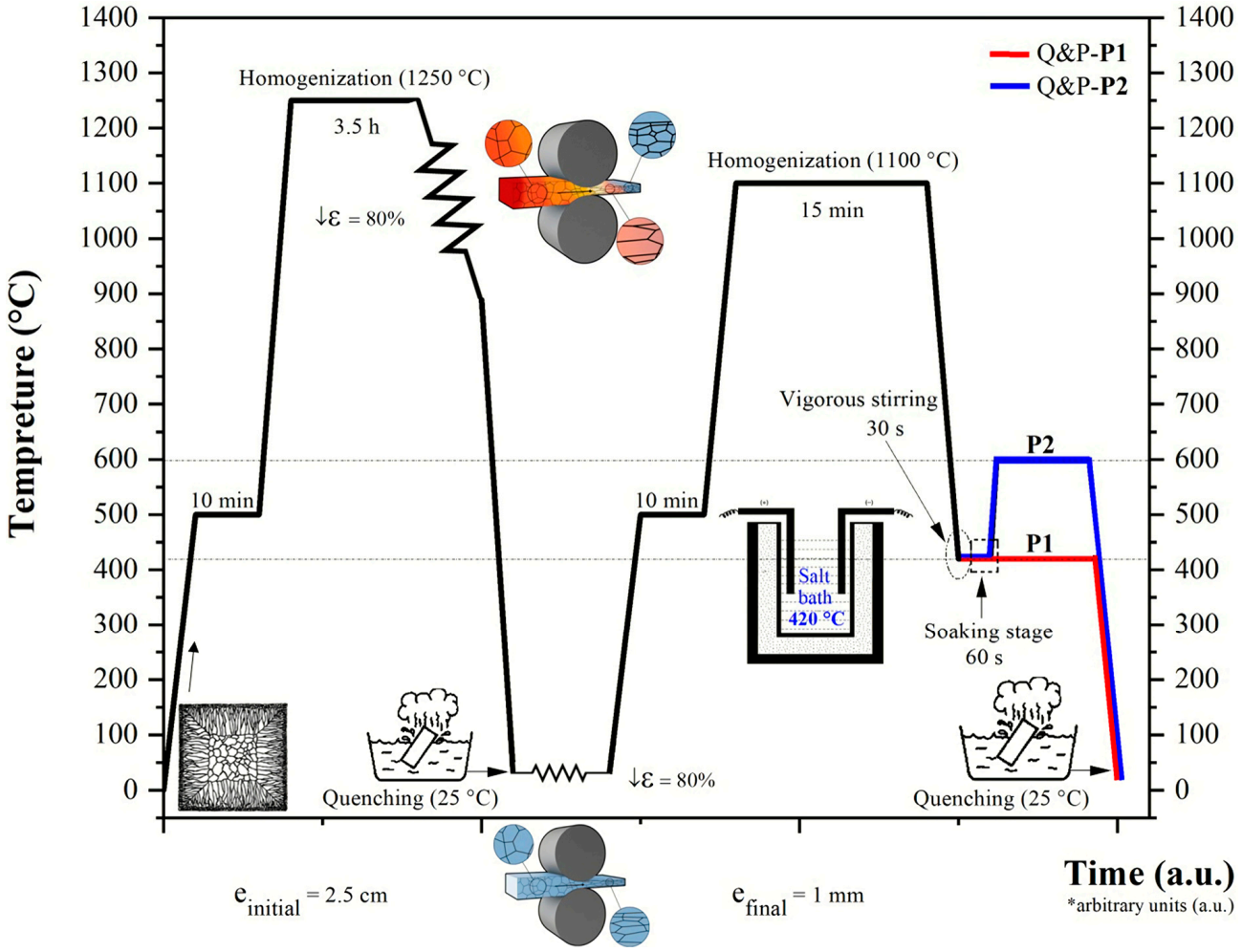

Figure 1. Complete thermo-mechanical, mechanical and thermal treatment for the microstructural evolution and conditioning of the boron-free (CP-B0) and boron-containing (CP-B60) steels, respectively.

The mechanical properties of the Q&P steels were determined by tension tests and microhardness measurements. In the case of the tension tests, a 10-ton load cell MTS QTEST/100 universal testing machine (MTS Systems Corporation, Eden Prairie, MI, USA) was used and operated at a head speed of 2 mm/min. For this purpose, rectangular mini-sub size samples as shown in Figure 2 were tested.

In the case of the microhardness measurements, the hardness profile was obtained from seven indentations in straight line, in which the indentations were separated by 100 μm. A Future Tech F11-7 microhardness tester (Shenyang TX Testing Instruments Inc., Hunnan District, Shenyang, China) was employed using a 100 g_f load and 10 s load time.

Finally, the corrosion resistance of the Q&P steels was evaluated by electrochemical tests. The surfaces of square samples of 20 mm × 20 mm by 1 mm thick were prepared for the tests employing monocrystalline 1 μm diamond paste. Once the required surface quality was achieved, the samples were placed into chemical cells set with a standard three electrodes arrangement (i.e., Q&P steel served as working electrode, a saturated calomel electrode (SCE) as a reference electrode and a graphite bar as a counter electrode). The opening of the cell in which samples were exposed to the 3% NaCl chemical solution was about 1.130 cm^2. The tests were carried out under an open circuit potential (OCP) and the relevant curves were obtained (i.e., potentiodynamic polarization curves) in a 1 mV/s data range. The values were plotted from −200 cathodic direction to 1200 mV anodic direction against the corrosion potential.

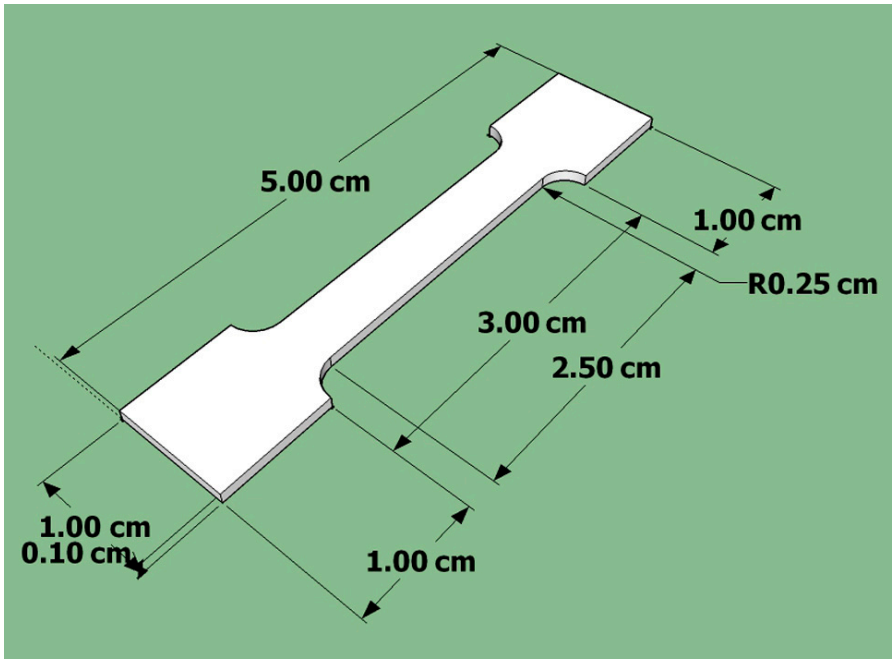

Figure 2. Dimensions of the tensile specimens.

3. Results and Discussion

3.1. Thermodynamical Equilibrium Calculations

Figure 3 shows the phase calculations for both boron-free (CP-B0) and boron-containing (CP-B60) steels. B can be seen to alter these diagrams as the temperature decreases from the liquid region to the solid one. The liquidus line starts at a value of 1499 °C in both steels, but the solidus line starts at 1440 °C for the boron-free steel and at 1417 °C for the boron-containing steel (see Figure 3a,b). This means that boron addition to the CP steel retards the solidification process by about 23 °C compared with the reference steel, leading to a wider two-phase (L+S) zone. According to Miettinen and Vassilev [17], the thermodynamic modelling of the Fe-B-X (X = Cr, Ni, Mn, Si, Ti, V, C) system, a Fe-B system, showed good correlation between phase transformation lines of simulated and experimental work. The computed equilibrium diagram for their work indicates how the mushy zone expands as boron content increase from 10^{-4} to 10^{-3} wt.% in the same way as it does in the present thermodynamical calculations for the highly-alloyed CP steel with 6×10^{-3} of boron content (i.e., 60 ppm of B). In addition, at a low weight percentage, second phase compounds are indicated in both diagrams of Figure 3a,b. In addition to the previous nitrides and carbonitrides compounds in the boron-free steel (see Figure 3c), new precipitates of boron (i.e., BN and M3B2) are formed (see Figure 3d). BN is precipitated at low weight percentages at 1327 °C and ends at 243 °C. It is evident that this harmful compound is present within the whole thermo-mechanical temperature range, including the straightening operation during the continuous casting operation. M3B2, the other boride precipitate, begins precipitation at 1006 °C and increases in concentration as the temperature decreases to room temperature. These two precipitates can affect the mechanical properties of steel in the same way as carbides by increasing the hardening of the material. Both of these precipitates can be detrimental to the hot ductility. Despite increasing the number of particles formed in steel, the volume fraction is still very small, presenting a percentage by weight of 0.074% as the maximum value. Because different B-rich compounds are formed during fabrication and subsequent processing of these steels and affect their properties in different ways, it is important to calculate and/or determine the temperatures of their formation, composition and volumetric fraction. It has been stated that if the deoxidation practice has been carried out properly, it is often preferred to use a sacrificial element, such as Ti, Si, Ce, Al or Zr, that forms less harmful precipitates when combined with nitrogen [18], thus increasing

the availability of free B in its atomic form so that it remains in solution in the steel matrix. However, when both oxygen and nitrogen levels are low, boron can precipitate in the form of boron carbides such as M3(B,C) (a type of boron-cementite) [19] and as Fe23(B,C)6 in the case of microalloyed steels with a low C content, both of which are less deleterious than BN. In the case of Fe23(B,C)6, the presence of elements such as Cr, Mo and Nb promotes the formation of the above indicated compound. Likewise, complex precipitates such as Fe23(B,C)6 can form around particles such as MnS or TiN itself [20]. Because they coarsen the particles and inclusions, the hot ductility is improved.

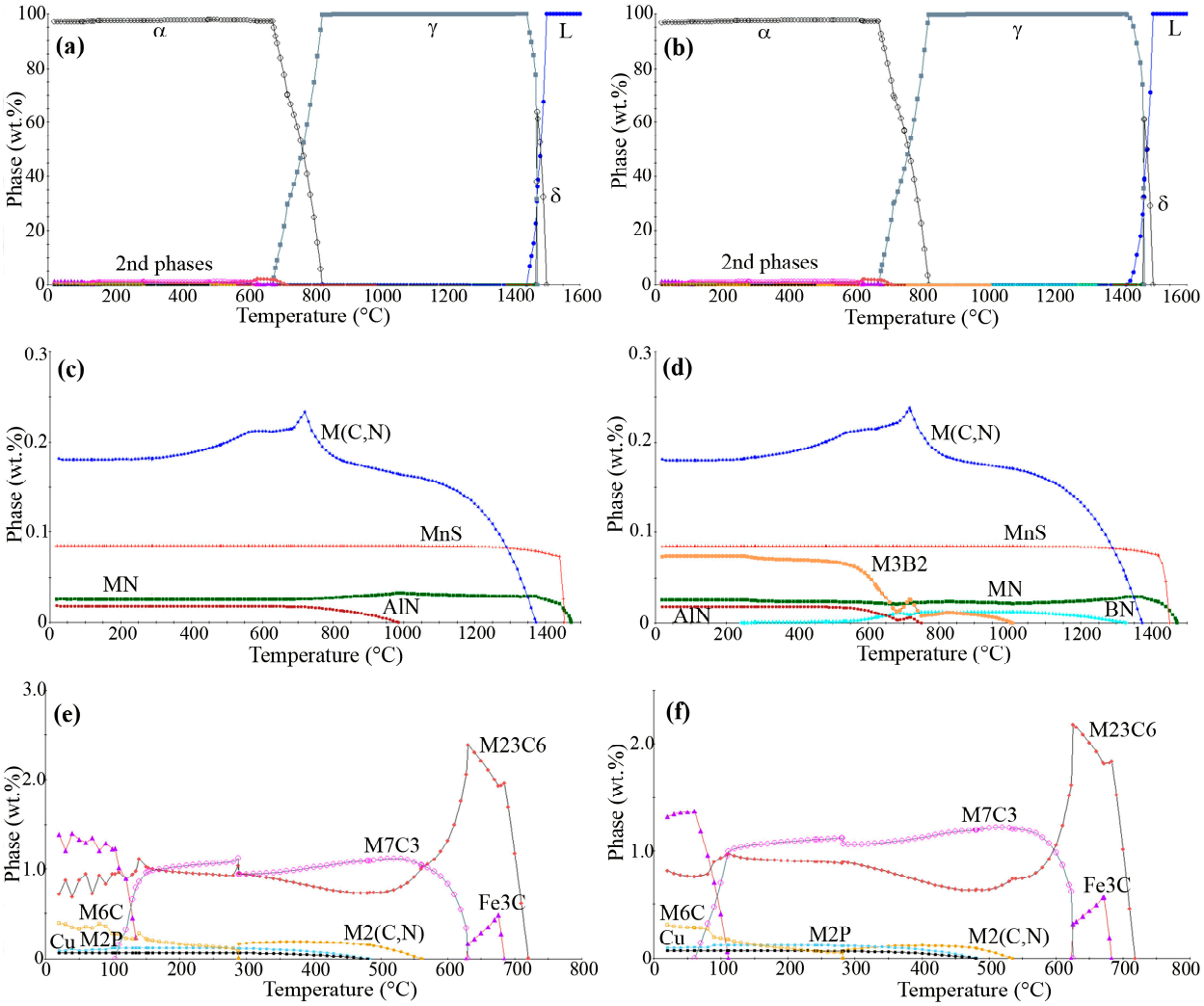

Figure 3. Weight percentage of the phases formed in the complex phase steel: (**a**,**c**,**e**) reference boron-free (CP-B0) steel, and (**b**,**d**,**f**) boron-containing (CP-B60) steel.

In the optimal range for B additions between 10 and 100 ppm, the different forms in which B can be found are: (a) boron precipitated as M23(B,C)6; (b) combined with N as BN; (c) as an interstitial element in solid solution; and (d) as an oxide, but usually in low amounts. Within the B range of 10 to 100 ppm, M23(B,C)6 is the most common form that can be found in steels with 0.05–0.25% C [21]. In the case when a heat treatment is carried out, the compound M23(B,C)6 usually manifests itself before the transformation from austenite to martensite, and this can act as a nucleation site for the formation of ferrite and even bainite [22]. For comparison purposes, these above-mentioned carbides are shown in Figure 3e,f as well as other important precipitates such as phosphides and complex copper compounds which can form. The presence of such precipitation will reduce ductility and toughness, especially when it is located at the grain boundaries.

3.2. X-ray Diffraction Study in the As-Cast Condition

Figure 4 shows the typical X-ray diffraction patterns of the boron-free complex phase (CP-B0) steel and boron-containing complex phase (CP-B60) steel after casting. It can be seen from Figure 4a,b that the predominant phase is α-ferrite. It is also noticeable that the amount of α-ferrite in the two diagrams is practically the same, unlike the diagram in Figure 4b where there is the presence of a γ-austenite peak from the (200) plane. This diffraction behavior is attributed to the effect of boron in stabilizing austenite and suppressing the transformation of γ-austenite to α-ferrite [20].

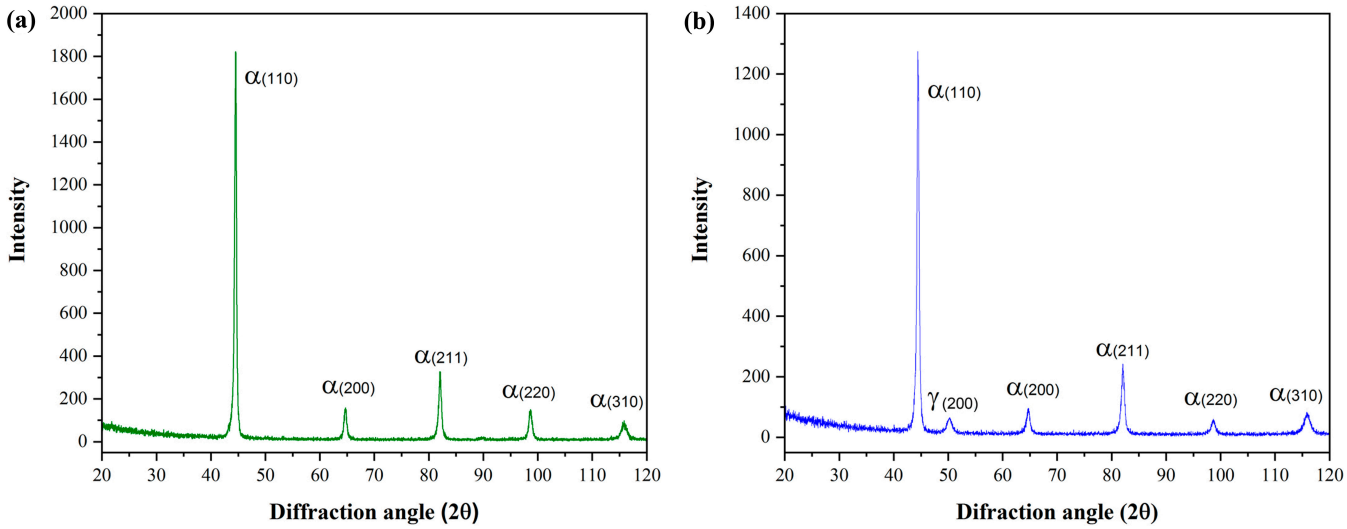

Figure 4. X-ray diffraction patterns of CP steels in the as-cast condition: (**a**) boron-free (CP-B0) steel, and (**b**) boron-containing (CP-B60) steel.

3.3. Grain Size Measurements in the As-Cast Condition

Figure 5a shows the average as-cast grain size values of the boron-free (CP-B0) and boron-containing (CP-B60) steels. It is evident that the grain size of the boron-containing steel is finer with an average value of 140 μm, compared with the boron-free steel with an average value of 206 μm. Furthermore, Figure 5b,d contains micrographs of the casting structure in the equiaxial zone of the CP-B0 and CP-B60 steels, respectively. Likewise, the SEM-EBSD IPF images are included in Figure 5c,e for the same steels in the columnar zone. In the IPF images, the solidification high-angle boundaries and the crystallographic orientation of grains can be observed. In the case of the boron-free steel, three competing preferred crystal orientations are observed, these being the (111), (001) and (122) planes. This crystal situation can account for the hot ductility behavior of the boron-free steel due to the resistance of each crystal to the strain during the straightening operation. As the crystals are bigger and more elongated, microcracks can easily nucleate, grow and propagate along the grain boundaries, resulting in low %RA values. On the other hand, only two preferred crystal orientations are observed in the boron-containing steel. These correspond with the predominant (112) plane and a remaining component in the (122) plane. Obviously, better hot ductility would be expected when the grain size is finer and linked with a more compatible crystal orientation to straining during the straightening operation. When a coarse solidification structure is obtained, the casting may suffer a decrease in its resistance to hot cracking, thereby affecting the hot workability and further decreasing the mechanical properties. Recently, it has been reported that in austenitic steels with high Mn content (TWIP steels), the microaddition of B has a refining effect on the cast structure, acting through an inoculant mechanism [10]. Additionally, it is highlighted that transition elements (e.g., Nb, Ti, Mo) also have an inoculant power and promote further refinement of the solidification granular structure of steel [23]. However, as the concentrations of these elements (Nb, Ti, Mo, etc.) are the same in both the CP-B0 and CP-B60 steels, it is assumed

that their presence will influence the precipitation kinetics and phase transformations in the same way and that the improvement in hot ductility can be attributed solely to the boron content in the CP steel.

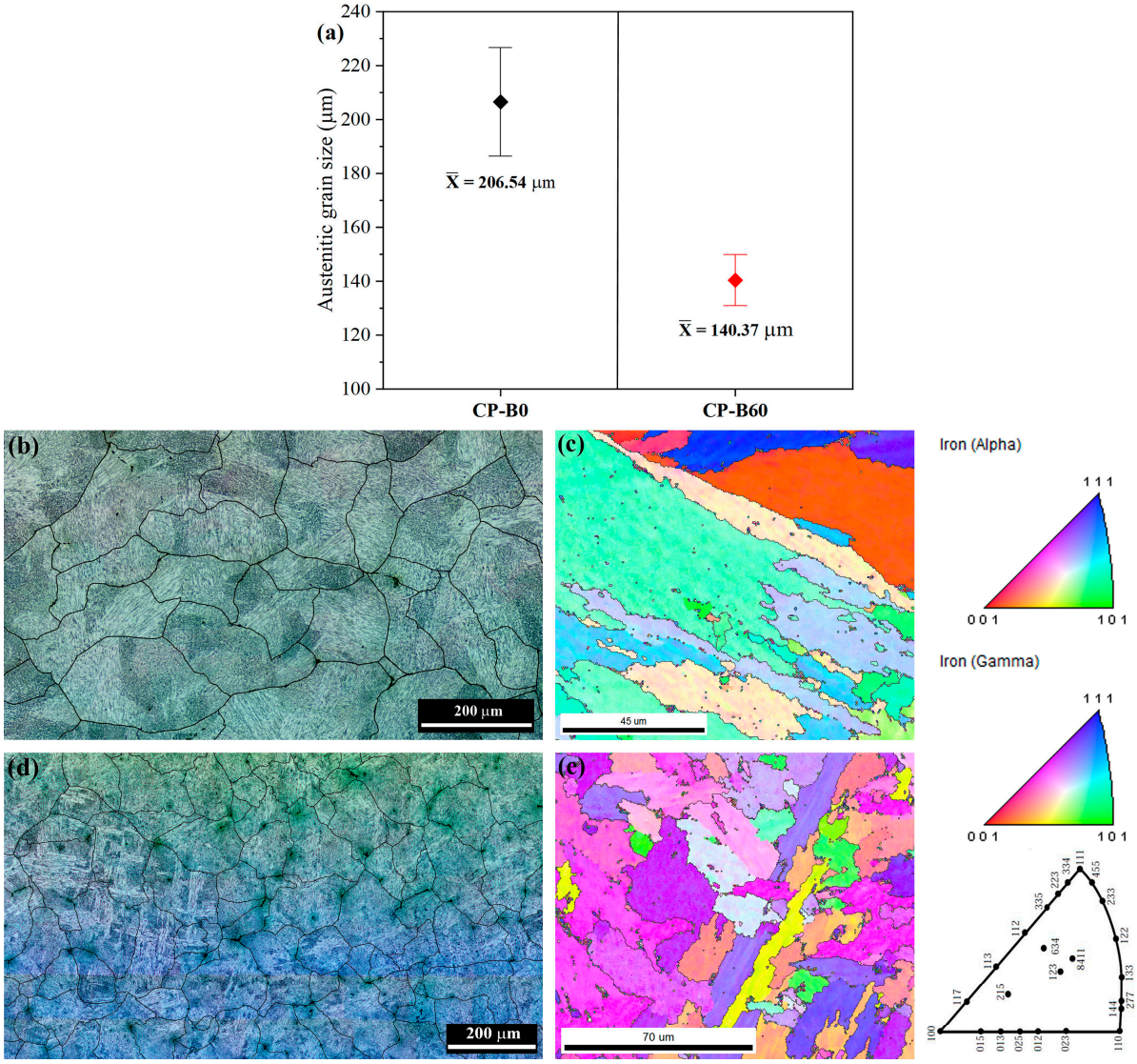

Figure 5. Solidification microstructure of the complex phase (CP) steel: (**a**) average profile of the austenitic grain size for boron-free (CP-B0) and boron-containing (CP-B60) steels, (**b**,**d**) optical micrographs of CP-B0 and CP-B60 steels, and (**c**,**e**) SEM-EBSD IPF images of CP-B0 and CP-B60 steels.

3.4. Hot Ductility Behavior

The hot ductility curves for these two CP steels plotted in terms of percent area reduction (%RA) versus test temperature are presented in Figure 6. The Ae_3 (upper equilibrium temperature between ferrite and austenite), Ar_3 and Ar_1 (starting and ending temperatures of the transformation of austenite to ferrite under continuous cooling) are also shown in this figure. The behavior is similar to that reported for all steels that undergo the austenite to ferrite transformation with the steels having a ductility trough in the temperature range 700 to 1000 °C [1,24]. It is clear from Figure 6 that the B-containing steel has the better ductility throughout the temperature range examined, particularly in the intermediate temperature range 775–875 °C. For both steels, there is a ductility trough, which mainly comprises the low-temperature region of γ-austenite, including the phase transformation zone from austenite to ferrite (γ→α), approximately from 750 to 850 °C, which corresponds to the range Ar_3 to Ae_3. The low ductility exhibited in this zone is

related to these softer ferrite films surrounding the harder austenite grains taking most of the strain and leading to low ductility along with ductile intergranular fracture at the austenite grain boundaries.

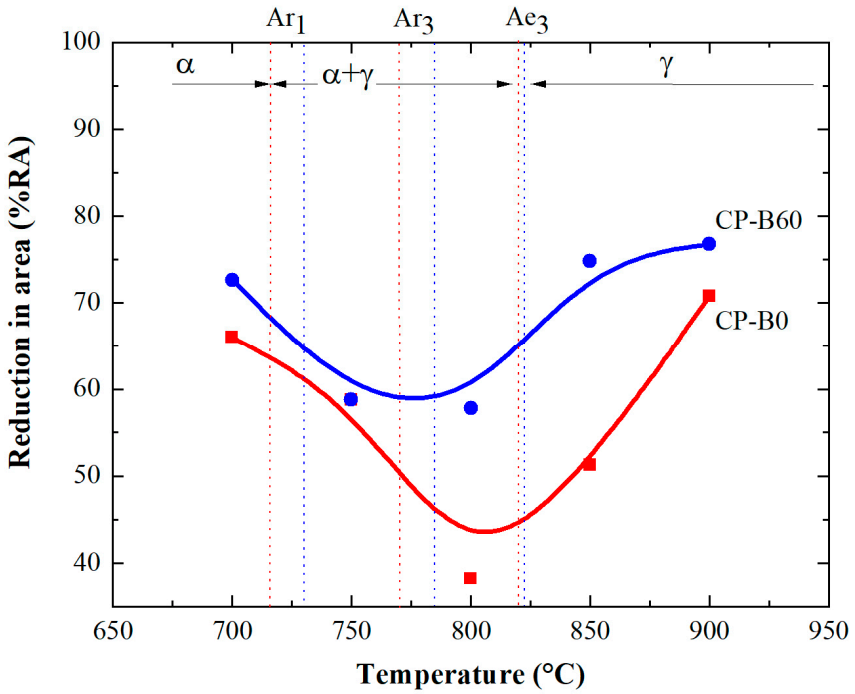

Figure 6. Hot ductility curves for the experimental advanced boron-free (CP-B0) and boron-containing (CP-B60) steels.

It is generally accepted that these thin films of strain-induced ferrite can form during cooling at temperatures above Ar_3 or even at higher temperatures such as Ae_3 [24–26]. This ferrite in the form of thin films of approximately 5 to 20 μm thick, being more ductile, acts in a similar way as precipitate-free zones, that is, it leads to a concentration of strain and consequently to a decohesion of the precipitates and inclusions located along the austenite grain boundaries. The boron-free (CP-B0) steel exhibits its lowest ductility at 800 °C with a value of 38% RA, and for this reason it would be marginally susceptible to transverse cracking during continuous casting or hot working. According to Mintz et al. [24], the critical temperature range in which RA is $\leq$ 40% is a highly sensitive range for transverse cracking on the steel surface during the straightening operation in the initial process of continuous casting. Hence, according to this criterion, the boron-free steel is susceptible to cracking, whereas the boron-containing steel should undergo the straightening operation without cracking. The better hot ductility behavior of the boron-containing steel is probably due to the boron retarding the transformation of pro-eutectoid ferrite. In previous investigations it has been shown that the primary or pro-eutectoid ferrite decreases proportionally with an increase in boron, leading to a substantial improvement in hot ductility [27]. However, another explanation is that given by Miller et al. [28] who suggest that the improved hot ductility of steels by boron additions is because the boron atoms act as a type of "adhesive or glue", preventing intergranular decohesion. In the same context, Laha et al. [29] proposed that boron segregating to grain boundaries alters the character of the grain–precipitate or matrix–precipitate boundary interface in such a way that it suppresses microcavity formation. As the temperature decreases below Ar_3 to within the inter-critical temperature range (γ+α), and before reaching Ar_1, the recovery of ductility at low temperatures is attributed to the increase in the volume fraction of α-ferrite [25,26]. In this case, the α-ferrite is no longer in the form of a thin layer surrounding the austenitic grain boundaries and, therefore, does not concentrate strains in these regions. Furthermore, the difference in resistance (strength) between α-ferrite and γ-austenite decreases with

decreases in the temperature, and plastic deformation in the austenite increases so that the strain is no longer localized.

In addition, since the α-ferrite is present in greater proportions and given its high stacking failure energy, the phenomenon of softening due to dynamic recovery is favored, leading to an increase in ductility. Similarly, the recovery of the ductility observed at high temperatures (above Ae_3, between 850 and 900 °C) is attributed to the disappearance of the thin layer of α-ferrite, so that there is no stress concentration at the grain boundaries that promotes intergranular fracture [24–26]. Additionally, at high temperatures, ductility improves thanks to the fact that the embrittlement mechanisms that could act in this temperature range such as precipitate-free zones and fine precipitates have ceased to exist. It is also considered that at high test temperatures (850–900 °C), the improvement of hot ductility by boron additions may be due to the coarsening of boron particles precipitated on austenitic grain boundaries so that dynamic recrystallization can occur. Yet another possible explanation for the improvement in hot ductility on adding boron is that boron produces coarse precipitation at the grain boundaries instead of fine precipitates within the matrix, thus reducing the stress acting on the grain boundaries [6,19].

Figure 7 shows the fracture appearance of CP steels tested at 700, 800 and 900 °C. Because ductility is generally good for even the boron-free steels ($\geq$40%), the fractures are ductile transgranular. However, intergranular failure is evident in the fracture appearance Figure 7c, of the boron-free steel tested at 800 °C which gave a RA value of 38%. The above discussion is nevertheless, in accordance with the observed fracture surface features, as explained in references [30–32].

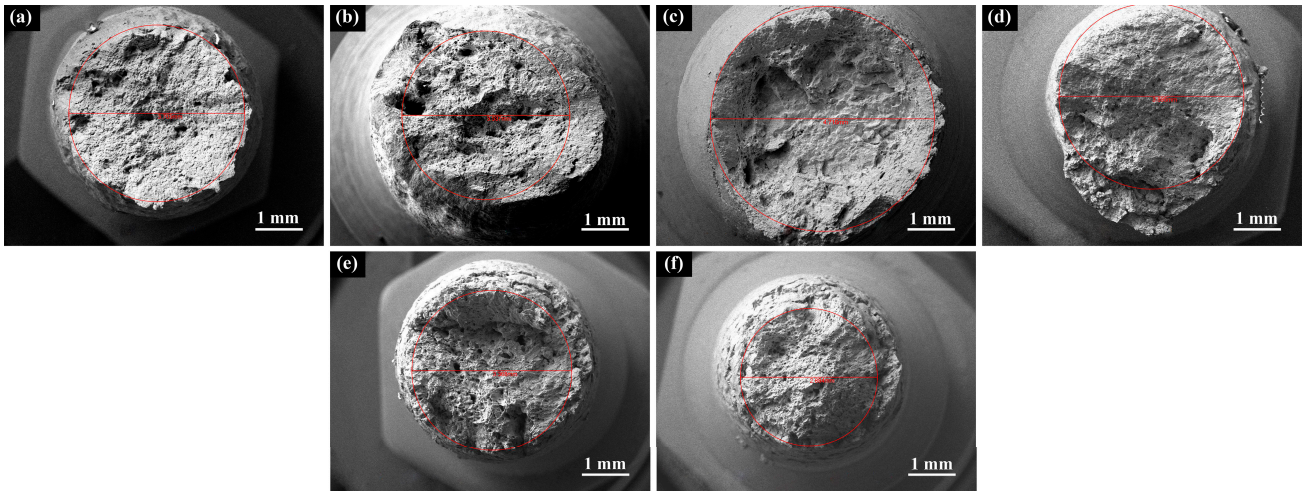

Figure 7. Fracture surface features obtained after hot testing: (**a**,**b**) boron-free (CP-B0) and boron-containing (CP-B60) steels tested at 700 °C, (**c**,**d**) CP-B0 and CP-B60 steels tested at 800 °C, and (**e**,**f**) CP-B0 and CP-B60 steels tested at 900 °C.

3.5. Analysis of the Martensitic Transformation

The theoretical equilibrium critical temperatures for the transformation of martensite from the JMatPro software are given in Figure 8. M_s is the temperature at which martensite begins to form, and M_f is the temperature at which the transformation from austenite to martensite is complete. The data obtained by the JMatPro program for the boron-free (CP-B0) steel indicates that the martensitic transformation (M_s) starts at 356 °C and the transformation ends (M_f) at a temperature of 241 °C. Additionally, it is indicated that M(50%) is at 321 °C. For the boron-containing (CP-B60) steel, the M_s, M_f and M(50%) are very similar, being 355, 240, 320 °C, respectively. However, there is a large difference in the hardenability, as the time available to harden the steel is extended from 10 to 50 s, as a consequence of the boron content (see Figure 8). The reason for the hardenability gain is probably that the boron atoms segregate to the grain boundaries of the austenite by a

non-equilibrium mechanism [33] linked to an extra effect of Nb and Mo content, moving to the right side the transformation lines in the TTT diagram. In consequence, the combined alloying of B, Nb and Mo is recognized as a synergetic effect on hardenability [34]. It is worthy to note that only the solid solution fraction of these elements can contribute to increasing hardenability.

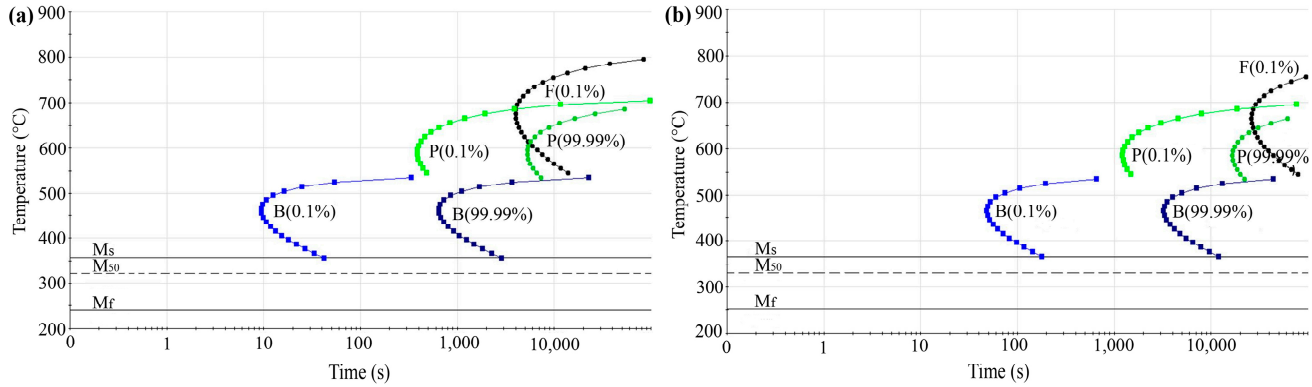

Figure 8. Hardenability curves obtained by JMatPro software: (**a**) CP-B0 steel and (**b**) CP-B60 steel.

In contrast, the experimental dilatometry curves shown in Figure 9 using a cooling rate of 200 °C/s give a very different data to the theoretical calculations. For the boron-free steel, the experimental M_s, M_f and M(50%) are 400, 240 and 335 °C, respectively. For the boron-containing steel, the experimental M_s, M_f and M(50%) are higher at 420, 300 and 360 °C, respectively.

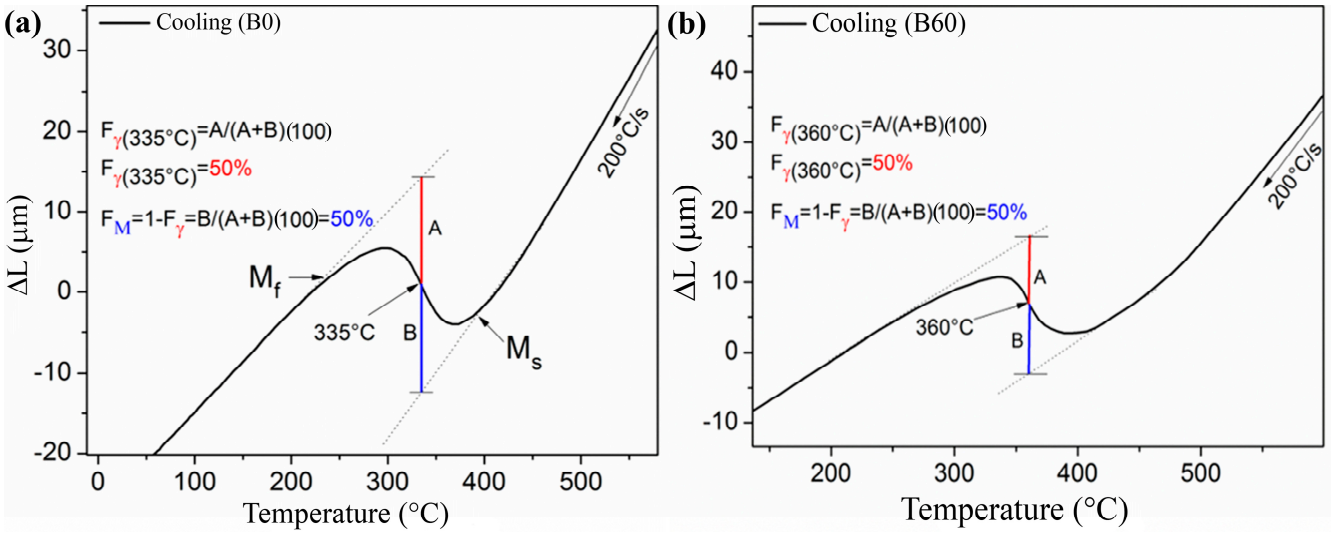

Figure 9. Experimental dilatometry curves for the martensitic transformation: (**a**) boron-free CP-B0 steel, and (**b**) boron containing CP-B60 steel.

This difference in behavior between the theoretical and experimental martensitic transformation data is probably because B suppresses the transformation from austenite to ferrite. The martensitic transformation temperature (M_s) is mainly a function of the amount of the various alloying elements and their concentration in solution in the austenite field. The M_s is normally only related to the composition of the steel. However, the M_s is also correlated to the austenitic grain size when the martensite phase begins to nucleate [35]. Martensite forms as packets or laths within austenite grains, and the number of detectable martensite packets per unit volume within the austenite is related to its grain size. If the austenite grain size is fine, there are more nucleation sites for the martensite nucleation and martensite can form more easily, resulting in a higher M_s value [36].

3.6. X-ray Diffraction Study of the Q&P Conditions

The X-ray diffraction patterns of the two steels after the partitioning heat treatments are given in Figure 10 (i.e., P1 and P2). The presence of the α-ferrite and γ-austenite phases can be seen in all cases. In the boron-containing steel for both partitioning treatments, P1 and P2, there is a greater presence of retained austenite (RA-γ) than in the boron-free steel, and in the P2 partitioning treatment of the Q&P treatment, there is a greater amount of RA-γ due to both the presence of boron and the quenching operation carried out above M_s., P2. In all cases, the austenite and ferrite peaks shown corroborate the presence of the AR-γ at room temperature. Furthermore, the two-step treatment generates the appearance of more phases in which the BCT structure (i.e., body-centered tetragonal unit cell) fits with the 14/mmm space group symmetry [37]. This BCT phase (i.e., untempered martensite) is formed as a consequence of partitioning quenching and reheating to 600 °C (P2), where its volumetric fraction grows at a higher temperature. Lu et al. [38] obtained a similar observation in their study of the Q&P treatment of a medium C steel. It is noted that the AR-γ obtained at higher temperatures during quenching is less stable due to the relatively high proportion of AR-γ so that there is insufficient C partitioning. Therefore, as a consequence of its low stability, it tends to decompose during the partitioning step, forming phases such as secondary ferrite or martensite.

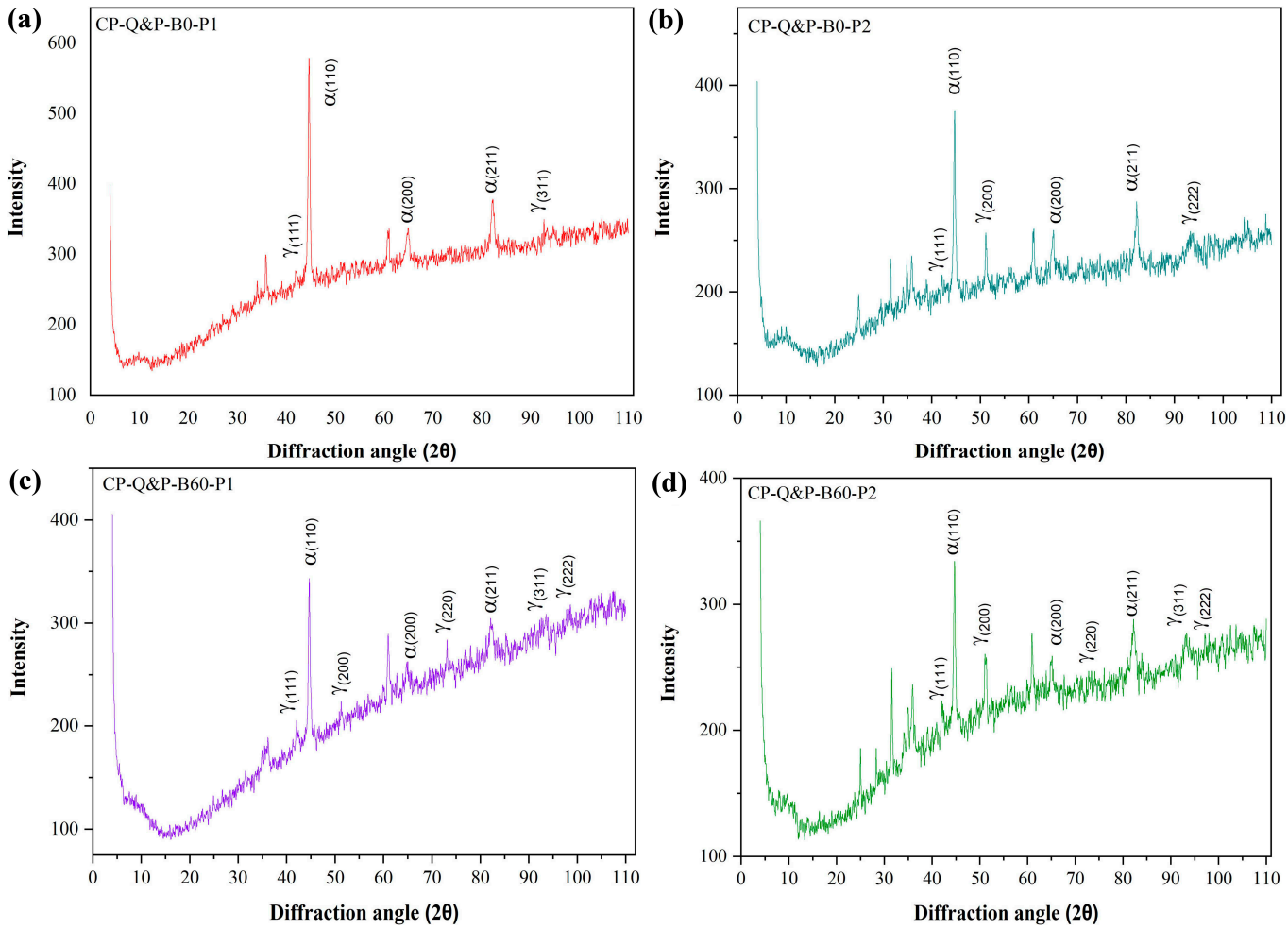

Figure 10. X-ray diffraction patterns of complex phase (CP) steels given the quenching and partitioning heat treatment (Q&P): (**a**) boron-free steel given partitioning treatment P1 (CP-B0-Q&P-P1), (**b**) boron-free steel given partitioning treatment P2 (CP-B0-Q&P-P2), (**c**) boron-containing steel given partitioning treatment P1 (CP-B60- Q&P-P1), and (**d**) boron-containing steel given partitioning treatment P2 (CP-B60-Q&P-P2).

3.7. Microstructural Characterization of CP Steels in the Q&P Conditions

In order to identify the microstructure of each steel after the heat treatment carried out using the concept of quenching and partitioning (Q&P), a first analysis was carried out by means of optical microscopy. Thanks to this, it was possible to identify the phases and microconstituents in the steels more easily. The microstructures that were obtained in the steels with each of the heat treatments yielded different morphologies of the microconstituents and phases, such as bainite, martensite, retained austenite, and ferrite. These constituents could be readily identified using the optical microscope, but the presence of pearlite was very difficult to distinguish due to the presence of bainite and the low carbon content of the steel. Its existence is assumed but in very minor quantities. Figure 11a shows the microstructure of the boron-free steel after the P1 partitioning route and indicates a bainitic matrix with large islands composed of RA-γ and, to a lesser extent, smaller ferrite islands. The morphology of the various microstructures is different. For example, RA-γ can be observed as a coarse and elongated in light brown color, appearing white in the image, whereas the α-ferrite is fine and has a bright, light color. Likewise, the dark layered regions correspond to martensite, which has the shape of laths, and the remaining microstructure with light brown and greenish colors corresponds to bainite, which is the matrix of steel. Figure 11b shows the microstructure after the two-step heat treatment for the boron-free steel (CP-B0-Q&P-P2) consisting of a fine grain structure immersed in a bainitic matrix, as well as martensite in ribbon shapes. Less martensite is retained in the two-step process due to the fact that when generating the second step, α-ferrite is formed and since there is no presence of boron, α-ferrite can be formed without any problem. It is also observed that there is a change in the morphology of the martensite needles generated after rapid cooling compared with the previous micrograph for the P1 treatment. Importantly, the two-step partitioning treatment leads to more RA-γ.

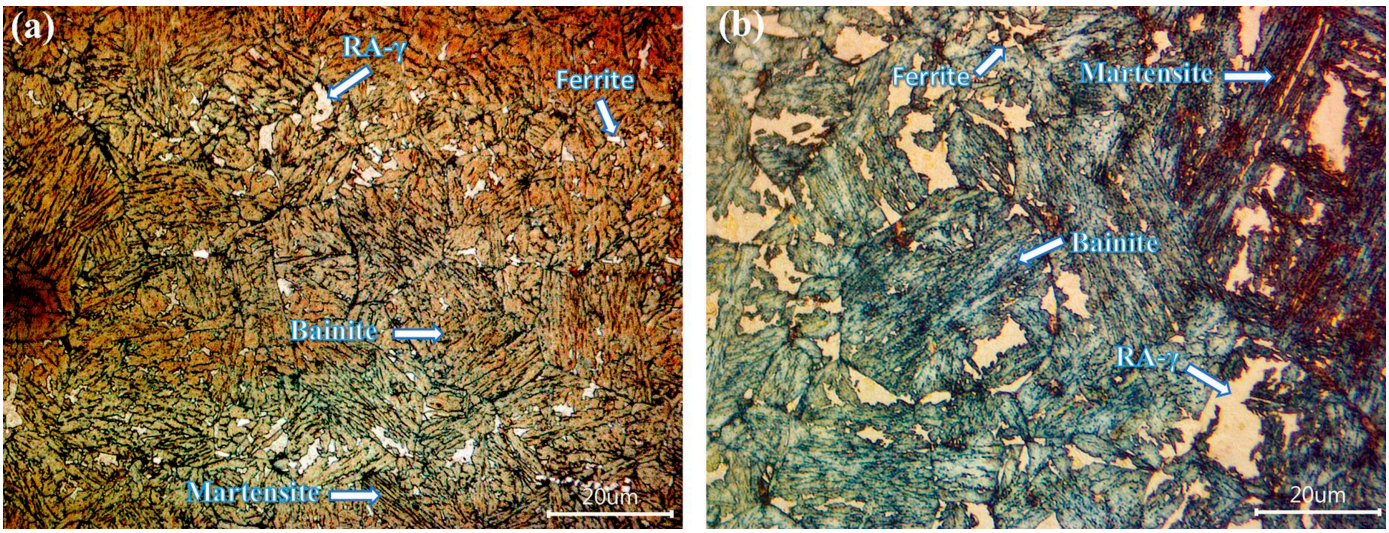

Figure 11. Q&P microstructure of (**a**) boron-free steel given the partitioning treatment P1 (CP-Q&P-B0-P1) and (**b**) boron-free steel given the partitioning treatment P2 (CP-Q&P-B0-P2). Optical microscope micrographs.

On adding boron there is even more RA-γ, as seen in Figure 12. In the same manner, Figure 12a shows the microstructure of the CP-B60 steel with the one-step heat treatment (CP-B60-Q&P-P1). This microstructure consists of a bainitic matrix in a pinkish brown color, and the martensite is in strips with a green hue. The morphology of the RA-γ, which is larger in size, can be seen with a light blue hue.

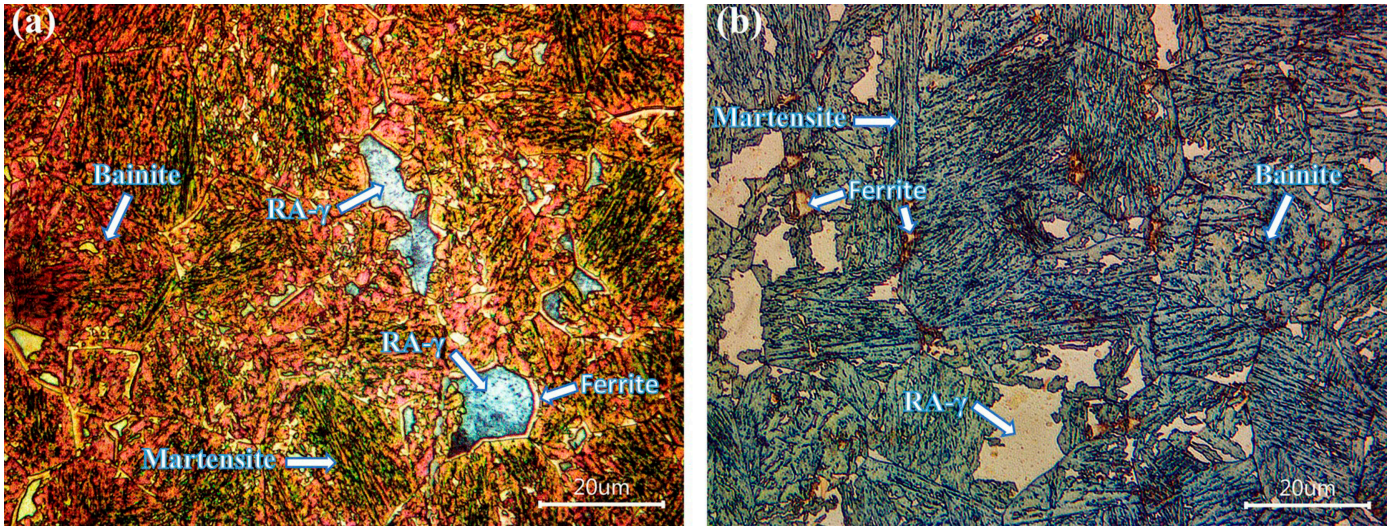

Figure 12. Q&P microstructure of (**a**) boron-containing steel given the partitioning treatment P1 (CP-Q&P-B0-P1) and (**b**) boron-containing steel given the partitioning treatment P2 (CP-Q&P-B60-P2). Optical microscope micrographs.

In addition, Figure 12b shows the microstructure, of the CP-B60-Q&P-P2 steel, which is very characteristic of a complex phase steel. The morphology of the phases and microconstituents is different from the previous conditions both in their distribution in the matrix as well as in the morphology of the RA-γ lakes, the martensite laths, the bainitic matrix and the α-ferrite.

The microstructures were examined in more detail using scanning electron microscopy (SEM). Figure 13 shows the Q&P microstructures of the P1- and P2-treated boron-free (CP-B0) and boron-containing (CP-B60) steels. The micrographs of the steels show a bainitic matrix (B) with a multiphase distribution typical of a complex phase (CP) steel, containing martensite (M), retained austenite (RA-γ) and ferrite (F). It is for this reason that the Q&P treatment is considered as a generator of multiphasic microstructures formed mainly by AR-γ and stabilized at room temperature, enriched with C and a hard phase such as martensite [39]. The main difference between the P1 and P2 partition routes in the Q&P treated, boron-free steels is the increase in the amount of martensite and retained austenite when the P2 route is used. In the case of the boron-containing Q &P treated steels, it can be seen from Figure 13c that the ferrite grows from retained austenite at the austenite grain boundaries, forming a film surrounding the retained austenite. However, the form is very different in the two-step P2 partition route, here the ferrite grows uniformly by the retained austenite transformation to ferrite (Figure 13d). These morphological changes in the microstructures of the Q&P steels have been conditioned by the influence of the initial solidification microstructure as well as the presence of boron and other microalloying elements that stabilize the austenite. It is important to mention that boron significantly affects the austenite field since boron tends to segregate at the grain boundaries, reducing the preferential sites for ferrite nucleation. In fact, this behavior causes a decrease in the interfacial energy and increases the temperature of the Ar_1 and Ar_3 transformation lines during cooling, which end up influencing the transformation kinetics of austenite in these bainitic–martensitic microstructures. Therefore, an improvement in toughness and ductility is expected.

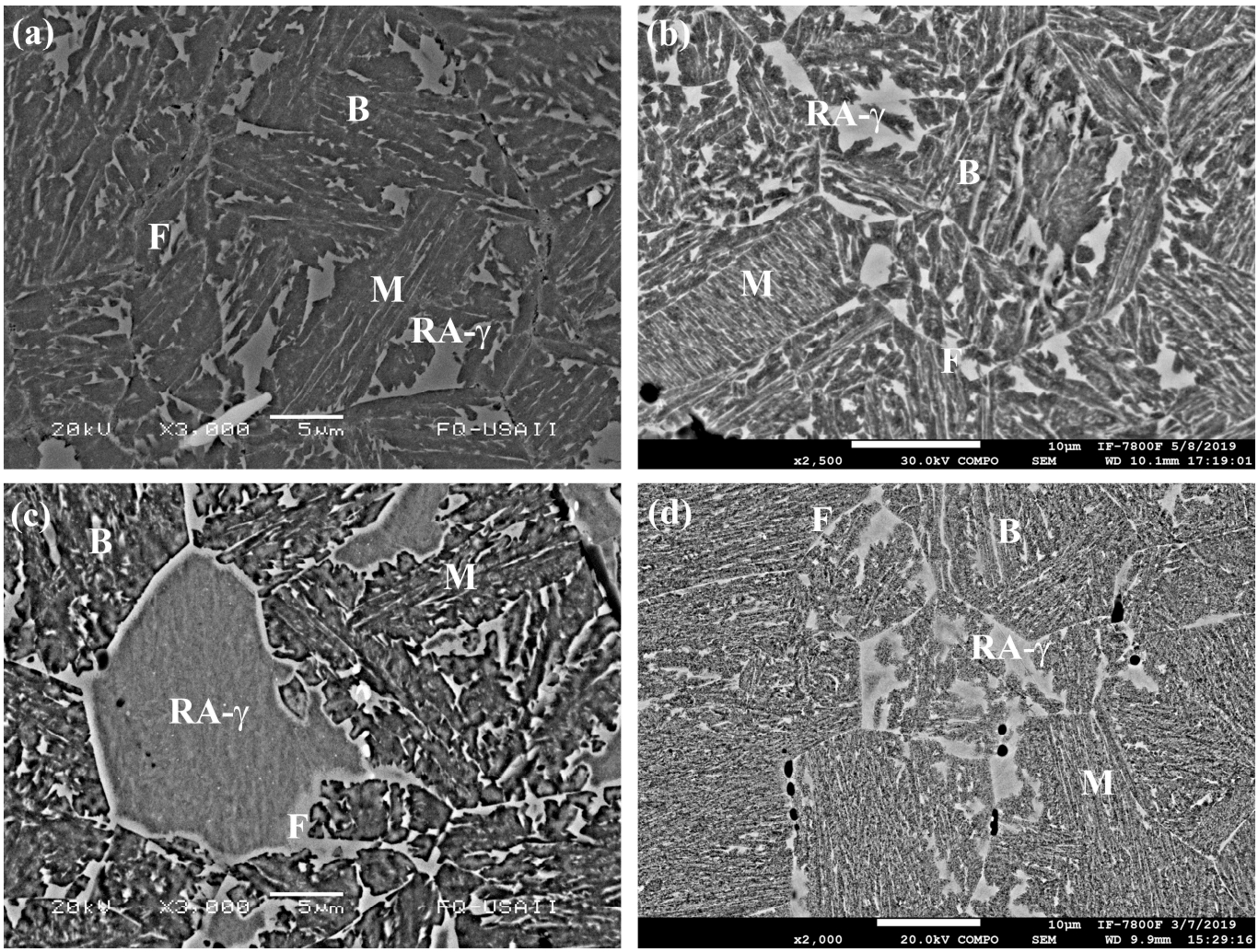

Figure 13. SEM micrographs of the microstructure of (**a**,**b**) boron-free steel given the Q&P treatment P1 and P2, respectively, and (**c**,**d**) boron-containing steel given the Q&P treatment P1 and P2, respectively.

The other observation that stands out is the effect of the partition route on the microstructural morphologies, as shown in Figure 14, i.e., the morphology of the AR-γ is very different for the one-step partitioning operation (P1) compared with that of the two-step process (P2). In addition to the presence of a more complex phase distribution, the morphology of the bainite (B) and martensite (M) is also observed to change in the boron treated steel. This change is attributed in the first instance to the effect of boron on stabilizing the austenite and suppressing the formation of ferrite and, secondly, to the thermal effect of the partitioning operation itself. In the specific case of the RA-γ, both the boron-free and boron-containing steels, CP-Q&P-B0 and CP-Q&P-B60, subjected to the one-step process (P1), show a block morphology, which is more noticeable in the boron-treated steel CP-Q&P-B60. In the case of the two-step process (P2), an acicular morphology of long islands is observed. Investigating this same concept of the different microstructural morphologies of RA-γ, Aoued et al. [37] observed the microstructural evolution during cooling and partitioning of a Fe-C-Mn-Si alloy model using image analysis. Based on the topological aspect of the phases as a first discrimination criterion, they identified and classified various morphologies of the retained austenite, bainite, and other BCT phases, and the morphologies obtained in this research work are very similar to theirs. Another important characteristic observed in the retained austenite, RA-γ is the presence of fine particles, possibly carbides, distributed in a homogeneous way. This phenomenon can be explained in terms of austenite carbon enrichment as the result of competitive reactions

such as martensite carbon partitioning, bainite transformation, and martensite carbon capture. Consequently, a significant part of the carbon enrichment that must happens in austenite can be attributed to the transformation of bainite.

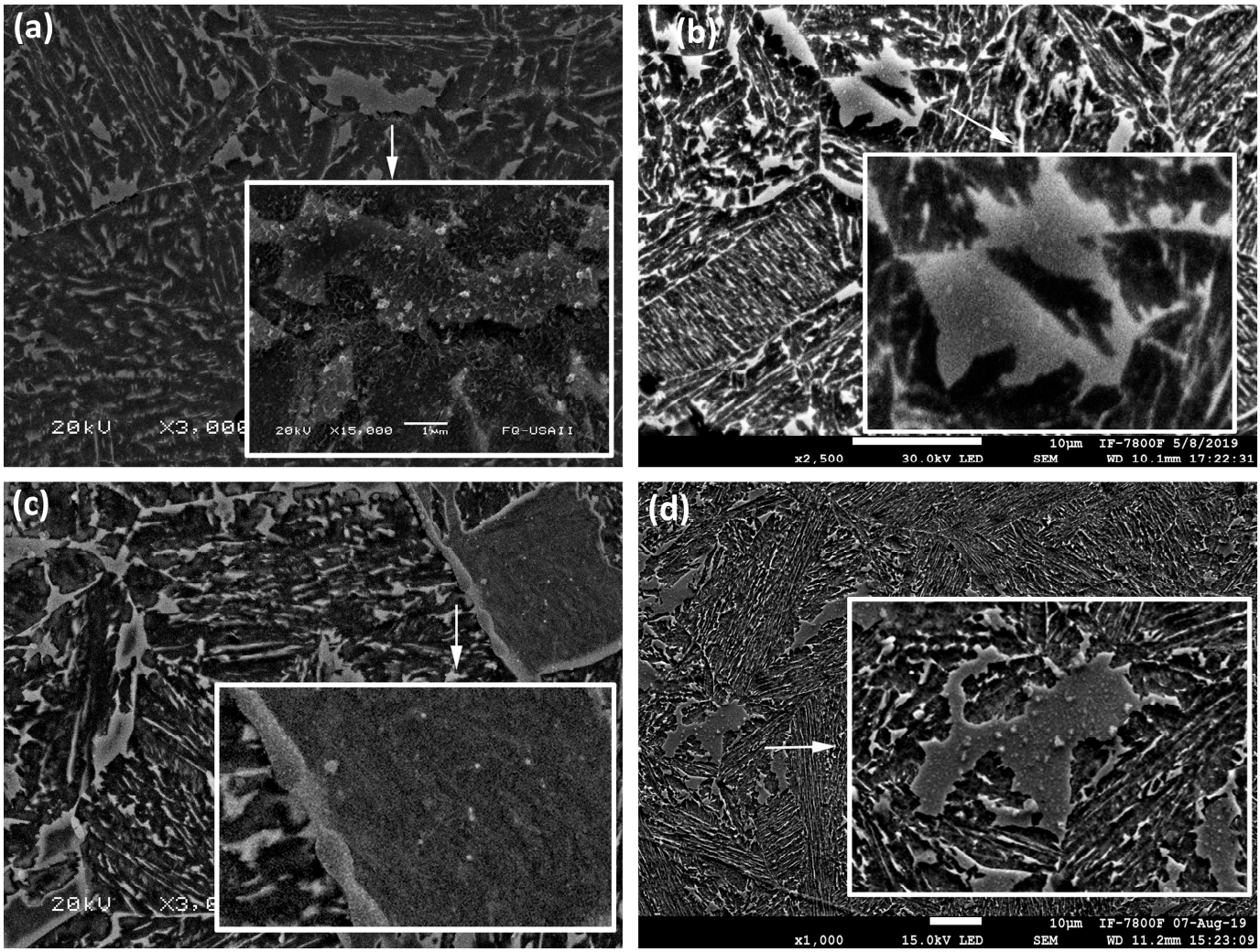

Figure 14. Micrographs showing the bainitic matrix and the morphology characteristics of the retained austenite (RA-γ) in (**a**) boron-free steel given the partitioning treatment P1 (CP-B0-Q&P-P1), (**b**) boron-free steel given the partitioning treatment P2 (CP-B0-Q&P-P2), (**c**) boron-containing steel given the partitioning treatment P1 (CP-B60-Q&P-P1), and (**d**) boron-containing steel given the partitioning treatment P2 (CP -B60-Q&P-P2).

3.8. Mechanical Characterization of CP Steels in the Q&P Conditions

Table 2 summarizes the results obtained after the uniaxial tensile test for the boron free and containing CP-B0 and CP-B60 steels given the Q&P heat treatment (P1 and P2). As can be seen, the best results, both in terms of mechanical resistance and elongation, were obtained in the CP steel microalloyed with boron. The two-step partitioning process P2 clearly gives improved mechanical properties, indicating that more partitioning of the C to the austenite takes place, resulting in a greater stabilization of the austenite. This means that the microstructural conditioning carried out on the steels has been good. Many other works that deal with this type of heat treatment also report improvements in mechanical properties [40–42] similar to those obtained in the present research work.

The stress-elongation curves of the boron-free steels, B0, subjected to the P1 and P2 steps, are shown in Figure 15a. It can be seen that the steels with the highest elongation percentages are produced when the Q&P treatment includes the two-step partitioning

process (B0-P2). It can be also appreciated from the curves that the work hardening rate is higher for the P2 partitioning route, leading to greater ductility. This behavior can be attributed to the presence of the softer microconstituents such as ferrite and retained austenite. The more brittle behavior and lower percentage of elongation obtained by the boron-free steel given the first step partitioning route, B0-P1, is due to the hard bainitic matrix, the presence of martensite and the reduced amount of retained austenite, as predicted by the design route that was taken (see the TTT diagrams) and confirmed by the experimental dilatometry data.

Table 2. Summary of the mechanical properties measured by means of uniaxial tensile tests of CP-B0 and CP-B60 steels produced in the Q&P treatment (P1 and P2).

Steel	Thickness (mm)	Width (mm)	Elongation (%)	YS (MPa)	UTS (MPa)
CP-Q&P-B0-P1	1.43	4.88	6.9	1090.4	1300.7
CP-Q&P-B0-P2	1.3	5.22	8.2	1074.1	1399.5
CP-Q&P-B60-P1	1.15	4.69	9.7	1055.7	1515.8
CP-Q&P-B60-P2	1.35	4.69	11.3	1212.2	1593.9

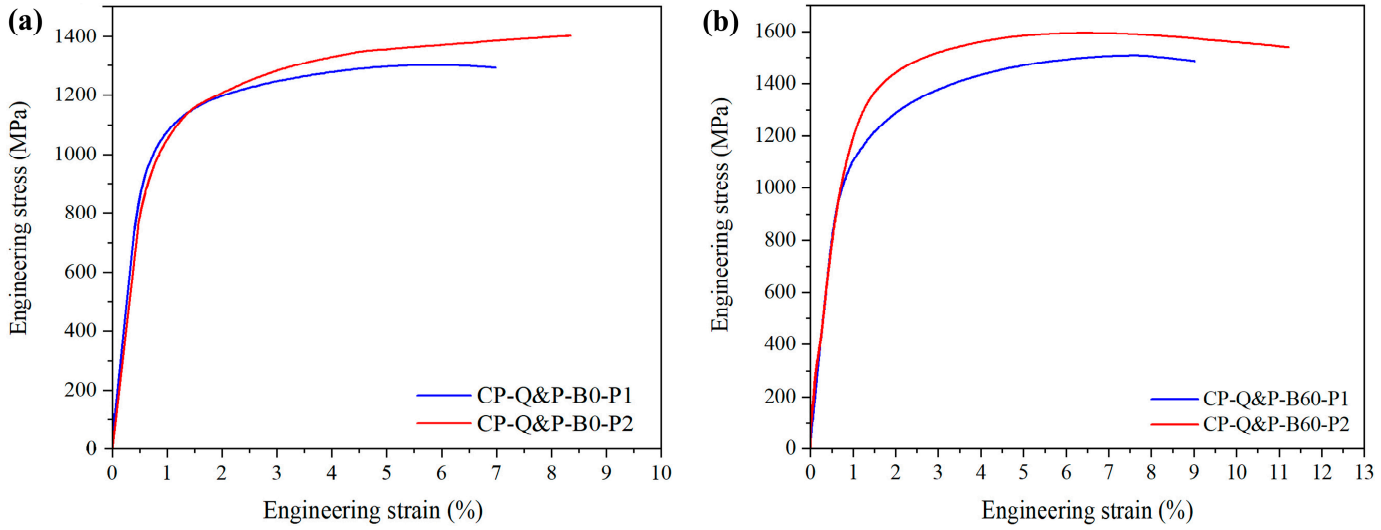

Figure 15. Engineering stress-strain curve for Q&P heat-treated CP steel with P1 and P2 steps: (**a**) boron-free (CP-Q&P-B0) steel, and (**b**) boron-containing (CP-Q&P-B60) steel.

However, the boron-treated steels give much better ductility as boron stabilizes the austenite. In the boron-treated steels, higher percentages of elongations are obtained for both partitioning routes, as seen in Figure 15b. This is due to the quenching and partitioning treatment that has the purpose of forming soft phases without affecting the other mechanical properties. This is attributed to the diffusion of carbon present in the martensite which enriches the retained austenite, thus increasing its ductility and toughness without affecting the other properties. Again, the second partitioning treatment gives the better ductility. As shown in the curves, the boron treated steel, given the first partitioning treatment P1 has a lower elongation than when given the second partitioning operation, P2. The boron treated steel, B60-P1 steel also has a higher strain hardening rate, and the yield strength decreases after reaching the maximum. Hence, the steel with the highest yield stress (YS) and maximum tensile strength (UTS) is the boron-treated steel given the second step partitioning, B60 P2, as shown in Table 2 and Figure 15b. The boron-containing steel given the P2 partitioning treatment has, considering its high strength, a substantial elongation percentage of 11%. This excellent combination of strength and ductility is due to the hard bainitic matrix being interspersed with soft ductile AR-γ and the soft α-ferrite phase.

It is also clear the alloying elements contribute to the strength of the final product. Many attempts have been made to link the tensile strength of the final product to its chemical composition. There are many formulae, but each equation accommodates a limited range of composition and does not take into account the thermal history of the steel. However, such formulae are useful to estimate the mechanical resistance of the final product when designing new steels. Mesplont [43] has reported, for example, an equation for CP AHSS steels based on their chemical composition to estimate the yield stress and UTS.

Microhardness measurements also seem to be a valid method for estimating the strength of these steels, although scatter tends to be high. Figure 16 shows the average hardness value for each heat treatment (Q&P of both P1 and P2) with and without the boron microaddition as well as their individual values. Compared with the boron-free steel, the boron-treated steel had higher average hardness values, approx. 40 VPN harder. For the boron-free steel, the two-step partitioning route produced a small increase in the average microhardness of approx. 10 VPN over the one-step partitioning treatment, but for the boron-treated steel, a substantial increase of approx. 40VPN compared to boron-free steel was observed, boron increasing the hardenability. However, it should be mentioned that the average microhardness values are high for all the steels due to the effect of the bainitic matrix that is present. It should also be noted that the increase in carbides and other fine precipitates due to boron increases the hardness of the steels, but the major cause is the effect boron has in increasing the hardenability. The use of empirical equations based on composition to calculate the strength [43] represents a very useful tool to design a steel with the required strength. These obtained mechanical properties in boron-containing Q&P steel treated by the two-step P2 partitioning route are within the parameters for its implementation in the automotive industry.

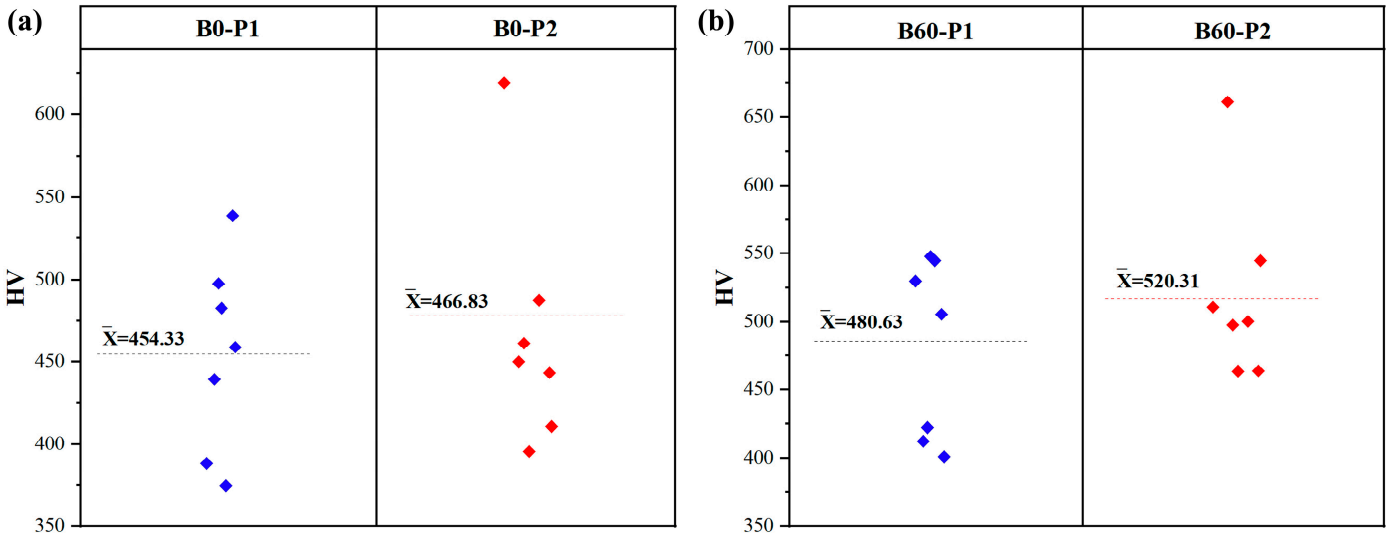

Figure 16. Vickers microhardness results for the complex phase (CP) steel heat-treated by the quenching and partitioning (Q&P) process: (**a**) boron-free steel produced by P1 and P2 steps, and (**b**) boron-containing steel produced by P1 and P2 steps.

3.9. Corrosion Characterization Behavior of CP Steels Produced under the Q&P Conditions

One of the major problems with these high strength CP steels is their corrosion resistance. The corrosion behavior of the samples was characterized using potentiodynamic polarization curves, and the results are shown in Figure 17a,b. The electrochemical parameters obtained from the polarization curves are summarized in Table 3. The plots show the typical features related to active behavior and the oxygen reduction reactions, evident in the anodic and cathodic regions, respectively. The active potential region is related to the dissolution of the alloy atoms into the solution, leading to an exponential current increase.

The transition of the active to the passive region is not evident, indicating that the specimen surfaces dissolved actively and were not covered by a protective corrosion products layer. The cathodic branch is associated with the oxygen reduction reaction. According to Strattman et al. [44], this reduction reaction is the most prominent in neutral and aerated NaCl solutions. The alloy composition and the process route of the steel samples (P1 or P2 routes) modify the reaction kinetics of the system.

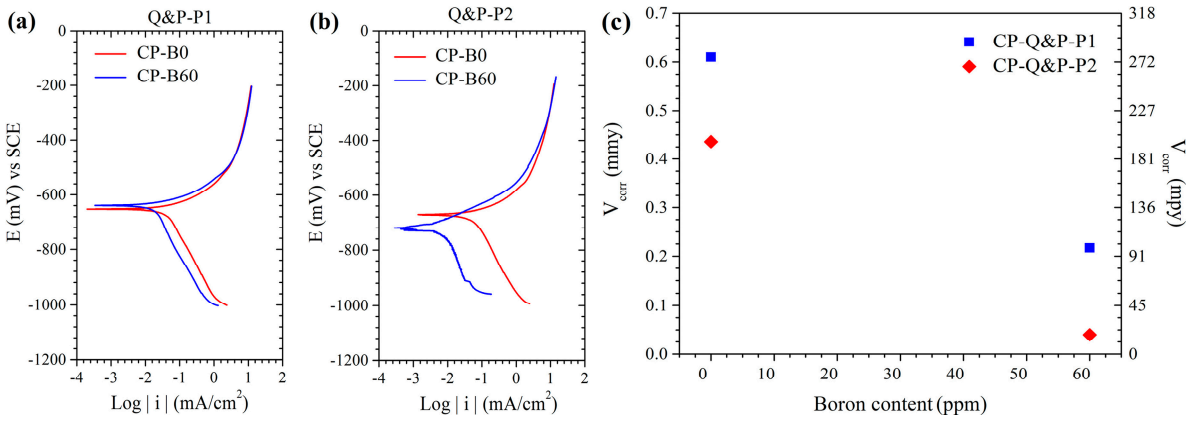

Figure 17. Polarization curves of the complex phase (CP) steel heat-treated by quenching and partitioning (Q&P) process: (**a**) boron-free steel with P1 and P2 steps, (**b**) boron-containing steel with P1 and P2 steps, and (**c**) influence of the concentration of B in the corrosion resistance of the CP-Q&P steels for P1 and P2 conditions.

Table 3. Characteristic parameters of the obtained polarization curves for CP-Q&P steels.

	CP-Q&P-P1		CP-Q&P-P2	
B Content (ppm)	**E_{corr} (mV vs. SCE)**	**I_{corr} (mA/cm^2)**	**E_{corr} (mV vs. SCE)**	**I_{corr} (mA/cm^2)**
0	−652	42.1	−670	45.3
60	−637.6	17.7	−717	7

For the one-step partitioning process (P1), the addition of B promotes a mixed behavior of the corrosion potential (E_{corr}) and the corrosion current (I_{corr}). In the case of the two-step P2 process, differences in the kinetics of the anodic and cathodic reactions are evident. Both reaction kinetics decrease as the content of B increase. The E_{corr} and the I_{corr} also decrease. For this case, the I_{corr} decreases around 85% with the boron addition, indicating that a synergic effect of the alloy composition and the P2 route enhances the corrosion resistance of the system.

This behavior can be attributed to the microstructural inhomogeneity of the samples with the presence of different amounts of crystalline phases. The different amounts of C in the composition of the phases as a consequence of the Q&P processes, leads to a galvanical effect between the martensite and RA-γ, due to the RA-γ acting as a cathode to the martensite [45]. As can be seen from the microstructures in Figures 11–14, the thermo-mechanical processing and the microaddition of B lead to the microstructure being modified, diminishing the amount of retained austenite and increasing the bainite and martensite fractions. The microstructural evolution (i.e., thermo-mechanical, mechanical and thermal treatment) and the addition of B to the CP steel showed a strong correlation with the enhancement of corrosion resistance, evidenced by the decrease in I_{corr}. The above-mentioned effects of both boron content and microstructural conditioning in the CP steel are summarized in Figure 17c. The corrosion rate was acquired using the method described by Yang et al. [46]. The plot shows an almost linear decrease in the corrosion rate of the sample with the increase in B content. This is in agreement with the results discussed above and with the work reported by Cetin who observed similar results in a 304 stainless steel [47].

4. Conclusions

(1) Although the experimental advanced complex phase (CP) steel was fabricated from scrap steel, the fabricated boron-free and boron-containing steels gave no processing problems (i.e., on solidification or during thermo-mechanical, mechanical and thermal treatment);

(2) The solidification grain size of the CP steel is refined by the boron addition from an average value of 207 μm for the boron-free steel to 140 μm for the boron-containing steel. The refining effect of B is attributed to an inoculation mechanism during the solidification process;

(3) The B addition to CP steel by refining the grain size improved the hot ductility, increasing the %RA value from 40 to 60 in the trough. However, the hot ductility for both the boron-free and boron-containing steels met the recommended RA values (i.e., >40%) needed to avoid cracking during the straightening operation in continuous casting of the steels although this was marginally so for the boron-free steel. Fracture surface features generally show ductile behavior. This hot ductility behavior indicates that the CP steel can probably be processed satisfactorily along the entire path of mechanical forming, with the addition of boron giving it added assurance;

(4) A bainitic matrix was always generated after the quenching and partitioning (Q&P) process, and within this matrix there were retained austenite (RA-γ) islands, martensite (M), bainite (B) and ferrite (F). In the case of the Q&P-P1 treatment, in both the boron-free and boron-containing steels, a RA-γ block morphology was observed, whereas for Q&P-P2, an acicular morphology of large islands of RA-γ were present. A surrounding layer of ferrite was also observed for the RA-γ of the boron treated steel given the P1 partitioning treatment;

(5) B improves the room temperature strength and ductility of these CP-Q&P steels. With only a small addition of 60 ppm of B, there is an equivalence of up to 10 times more carbon in the retained austenite, producing a more stable retained austenite and leading to better ductility and strength. With this boron addition to the CP steel, the UTS increases by 200 MPa for both the P1 and P2 partitioning routes. Changing the partitioning route from one to two steps results in an approx. 100 MPa increase in UTS for both the boron-free and boron-containing steels. Hence, the greatest benefit comes with a boron addition and the P2 partitioning route so that a YS of 1212 MPa and UTS of 1594 MPa were achieved;

(6) The B addition improves the corrosion resistance in the advanced complex phase (CP) steel when heat-treated using the quenching and partitioning (Q&P) process. The B addition gives a better distribution of the phases and carbon contents lead to less galvanic reaction. The P2 route by going to a higher partitioning temperature of 600 °C relieves the internal stresses and so improves the corrosion resistance. Again, the boron-containing CP steel given the two-step partitioning process (P2) has the greatest corrosion resistance of all the examined conditions.

Author Contributions: Conceptualization, A.E.S.-R., G.A.-G., B.M. and A.S.; funding acquisition, A.E.S.-R.; investigation, A.E.S.-R., G.A.-G. and J.R.G.-P.; methodology, A.S., G.L.-R., I.A.F., J.R.G.-P. and R.D.; writing—original draft, A.E.S.-R.; writing—review and editing, G.A.-G., J.R.G.-P. and B.M. All authors have read and agreed to the published version of the manuscript.

Funding: This research work was supported by the Programa de Apoyo a la Investigación y el Posgrado (PAIP—5000-9168)—Faculty of Chemistry (FQ)—UNAM.

Acknowledgments: The authors are grateful for the valuable technical support of Federico Chávez Alcalá for the fabrication of the complex phase (CP) steel (DIM—IPN). The Department of Metallic Materials of the Materials Research Institute (IIM)—UNAM, the Department of Materia Condensada of the Physics Institute (IF)—UNAM and the Department of Mechanical Testing—CINVESTAV—Unidad Saltillo are acknowledged for the technical assistance in carrying out experimental characterization techniques. In addition, the authors are grateful for the valuable technical support of Fernando Daniel Acevedo Sanchez (DIM—FQ—UNAM), Horacio Rodríguez Santillán (DIM—FQ—UNAM), José

Fernando Flores Álvarez (DIM—FQ—UNAM), Agustin Gerardo Ruíz Tamayo (DIM—FQ—UNAM), Gerardo Arámburo Pérez (FQ-UNAM), Sergio García Galán (DIM—FQ—UNAM), Adriana Tejeda (IIM—UNAM), José Reyes Gasga (IF—UNAM), Samuel Tehuacanero Nuñez (IF—UNAM), Samuel Tehuacanero Cuapa (IF—UNAM), Antonio Morales Espino (IF—UNAM), Diego Armando Quiterio Vargas (IF—UNAM) and Pablo López (IF—UNAM).

Conflicts of Interest: The authors declare no conflict of interest.

References

1. Mintz, B.; Crowther, D.N. Hot ductility of steels and its relationship to the problem of transverse cracking in continuous casting. *Inter. Mater. Rev.* **2010**, *55*, 168–196. [CrossRef]
2. Brune, T.; Senk, D.; Walpot, R.; Steenken, B. Hot ductility behavior of boron containing microalloyed steels with varying manganese content. *Metal. Mater. Trans. B* **2015**, *46*, 1400–1408. [CrossRef]
3. Komenda, J.; Martin, D.; Lönnqvist, J. The effect of boron addition on precipitation and hot ductility of 1.5Mn-0.1Nb-Ti carbon steels in as-cast condition. *Mater. Sci. Forum* **2016**, *879*, 990–995. [CrossRef]
4. Komenda, J.; Luo, C.; Lönnqvist, J. Interaction of carbon, titanium, and boron in micro-alloy steels and its effect on hot ductility. *Alloys* **2022**, *1*, 133–148. [CrossRef]
5. Li, Q.; Liu, W. Effect of boron on hot ductility and room-temperature tensile properties of microalloyed steels with titanium and niobium. *Materials* **2019**, *12*, 2290. [CrossRef]
6. Mejía, I.; Altamirano, G.; Bedolla-Jacuinde, A.; Cabrera, J.M. Effect of boron on the hot ductility behavior of a low carbon advanced ultra-high strength steel (A-UHSS). *Metall. Mater. Trans. A* **2013**, *44*, 5165–5176. [CrossRef]
7. Kang, S.E.; Banerjee, J.R.; Maina, E.M.; Mintz, B. Influence of B and Ti on the hot ductility of high Al and high Al, Nb containing TWIP steels. *Mater. Sci. Technol.* **2013**, *29*, 1225–1232. [CrossRef]
8. Kang, S.E.; Banerjee, J.R.; Tulin, A.S.; Mintz, B. Influence of B on hot ductility of high Al, TWIP steels. *Mater. Sci. Technol.* **2014**, *30*, 486–494. [CrossRef]
9. Mejía, I.; Salas-Reyes, A.E.; Calvo, J.; Cabrera, J.M. Effect of Ti and B microadditions on the hot ductility behavior of a high-Mn austenitic Fe-23Mn-1.5Al-1.3Si-0.5C TWIP steel. *Mater. Sci. Eng. A* **2015**, *648*, 311–329. [CrossRef]
10. Salas-Reyes, A.E.; Altamirano-Guerrero, G.; Chávez-Alcalá, J.F.; Barba-Pingarrón, A.; Figueroa, I.A.; Bolarín-Miró, A.M.; Sánchez-De Jesús, F.; Deaquino-Lara, R.; Salinas, A. Influence of boron content on the solidification structure, magnetic properties and hot mechanical behavior in an advanced as-cast TWIP steel. *Metals* **2020**, *10*, 1230. [CrossRef]
11. Raabe, D.; Sun, B.; Kwiatkowski Da Silva, A.; Gault, B.; Yen, H.W.; Sedighiani, K.; Thouden-Sukumar, P.; Souza-Filho, I.R.; Katnagallu, S.; Jägle, E.; et al. Current challenges and opportunities in microstructure-related properties of advanced high-strength steels. *Metall. Mater. Trans. A* **2020**, *51*, 5517–5586. [CrossRef]
12. Speer, J.G.; Matlock, D.K.; De Cooman, B.C.; Schroth, J.G. Carbon partitioning into austenite after martensite transformation. *Acta Mater.* **2003**, *51*, 2611–2622. [CrossRef]
13. Speer, J.G.; Edmonds, D.V.; Rizzo, F.C.; Matlock, D.K. Partitioning of carbon from supersaturated plates of ferrite, with application to steel processing and fundamentals of the bainite transformation. *Curr. Opin. Solid State Mater. Sci.* **2004**, *51*, 2611–2622. [CrossRef]
14. Li, Y.J.; Liu, D.; Zhang, W.N.; Kang, J.; Chen, D.; Yuan, G.; Wang, G.D. Quenching above martensite start temperature in quenching and partitioning (Q&P) steel through control of partial phase transformation. *Mater. Lett.* **2018**, *230*, 36–39.
15. Pashangeh, S.; Somani, M.; Ghasemi-Banadkouki, S.S. Structure-property correlations of a medium C steel following quenching and isothermal holding above and below the M_s temperature. *ISIJ Int.* **2021**, *61*, 442–451. [CrossRef]
16. Yang, J.; Lu, Y.; Guo, Z.; Gu, J.; Gu, C. Corrosion behavior of a quenched and partitioned medium carbon steel in 3.5 wt.% NaCl solution. *Corros. Sci.* **2018**, *130*, 64–75. [CrossRef]
17. Miettinen, J.; Vassilev, G. Thermodynamic description of ternary Fe-B-X systems. Part 2: FeB-Ni. *Arch. Metall. Mater.* **2014**, *59*, 609–614. [CrossRef]
18. Werner, D.W. *Boron and Boron Containing Steels*; Verlag Stahleisen mbH: Dusselfdorf, Germany, 1995.
19. Watanabe, S.; Ohtani, H.; Kunitake, T. The influence of hot rolling and heat treatment on the distribution of boron in steels. *Trans. ISIJ* **1983**, *23*, 31–37. [CrossRef]
20. Sharma, M.; Ortlepp, I.; Bleck, W. Boron in heat-treatable steels: A review. *Steel Res. Int.* **2019**, *90*, 1900133. [CrossRef]
21. López-Chipres, E.; Mejía, I.; Maldonado, C.; Bedolla-Jacuinde, A.; Cabrera, J.M. Hot ductility behavior of boron microalloyed steels. *Mater. Sci. Eng. A* **2007**, *460–461*, 464–470. [CrossRef]
22. Yamanaca, K.; Ohmori, Y. Effect of boron on transformation of low-carbon low-alloy steels. *J. Iron Steel Inst. Jpn.* **1976**, *62*, 895–904. [CrossRef]
23. Kurtz, R.A. Grain Refinement in Steel Castings. Master's Thesis, Massachusetts Institute of Technology, Cambridge, MA, USA, 1960.
24. Mintz, B.; Yue, S.; Jonas, J.J. Hot ductility of steels and its relationship to the problem of transverse cracking during continuous-casting. *Inter. Mater. Rev.* **1991**, *36*, 187–217. [CrossRef]

25. Mintz, B. The influence of composition on the hot ductility of steels and to the problem of transverse cracking. *ISIJ Int.* **1999**, *39*, 833–855. [CrossRef]
26. Mintz, B.; Jonas, J.J. Influence of strain-rate on production of deformation-induced ferrite and hot ductility of steels. *Mater. Sci. Technol.* **1994**, *10*, 721–727. [CrossRef]
27. Mintz, B. Importance of Ar3 temperature in controlling ductility and width of hot ductility trough in steels, and its relationship to transverse cracking. *Mater. Sci. Technol.* **1996**, *12*, 132–138. [CrossRef]
28. Miller, M.K.; Pareige, P.J.; Russell, K.F. Seeing and Catching Atoms. In *An Oak Ridge National Laboratory Report*; Oak Ridge National Laboratory: Oak Ridge, TN, USA, 2001.
29. Laha, K.; Kyono, J.; Sakai, T.; Kishimoto, S.; Shinya, N. Austenitic stainless steel through the self-healing effect of boron for creep cavitation. *Metall. Mater. Trans. A* **2005**, *36*, 399–409. [CrossRef]
30. Liu, Y.; Du, L.X.; Wu, H.Y.; Misra, R.D.K. Hot ductility and fracture phenomena of low-carbon V-N-Cr microalloyed steels. *Steel Res. Int.* **2019**, *91*, 1900265. [CrossRef]
31. Salas-Reyes, A.E.; Mejía, I.; Bedolla-Jacuinde, A.; Boulaajaj, A.; Calvo, J.; Cabrera, J.M. Hot ductility behavior of high-Mn austenitic Fe-22Mn-1.5Al-1.5Si-0.45C TWIP steels microalloyed with TI and V. *Mater. Sci. Eng. A* **2014**, *611*, 77–89. [CrossRef]
32. Wang, X.M.; He, X.L. Effect of boron addition on structure and properties of low carbon bainitic steels. *ISIJ Inter.* **2002**, *42*, S38–S46. [CrossRef]
33. Zurutuza, I.; Isasti, N.; Detemple, E.; Schwinn, V.; Mohrbacher, H.; Uranga, P. Effect of Nb and Mo additions in the microstructure/tensile property relationship in high strength quenched and quenched and tempered boron steels. *Metals* **2021**, *11*, 29. [CrossRef]
34. Yoshida, S.; Ushioda, K.; Agren, J. Knetic modelo f the γ to α phase transformation at grain boundaries on boron-bearing low-alloy steel. *ISIJ Int.* **2014**, *54*, 685–692. [CrossRef]
35. Lee, S.J.; Lee, Y.K. Effect of austenite grain size on martensitic transformation of a low alloy steel. *Mater. Sci. Forum* **2005**, *475-479*, 3169–3172. [CrossRef]
36. Celada-Casero, C.; Sietsma, J.; Santofimia, M.J. The role of the austenitic grain size in the martensitic transformation in low carbon steels. *Mater. Des.* **2019**, *167*, 107625. [CrossRef]
37. Aoued, S.; Danoix, F.; Allain, S.; Gaudez, S.; Geandier, G.; Hell, J.C.; Soler, M.; Gouné, M. Microstructure evolution and competitive reactions during quenching and partitioning of a model Fe-C-Mn-Si alloy. *Metals* **2020**, *10*, 137. [CrossRef]
38. Lu, J.; Yu, H.; Kang, P.; Duan, X.; Song, C. Study of microstructure, mechanical properties and impact-abrasive wear behavior of medium-carbon steel treated by quenching and partitioning (Q&P) process. *Wear* **2018**, *414–415*, 21–30.
39. Bigg, T.D. Quenching and Partitioning: A New Steel Heat Treatment Concept. Ph.D. Thesis, The University of Leeds, Leeds, UK, 2011.
40. Entezari, E.; Mousalou, H.; Yazdani, S.; González-Velázquez, J.L.; Szpunar, J.A. The evaluation of quenching temperature effect on microstructural and mechanical properties of advanced high strength low carbon steel after quenching partitioning treatment. *Procedia Struct. Integr.* **2022**, *37*, 145–152. [CrossRef]
41. Bai, B.; Gao, G.; Gui, X.; Tan, Z.; Weng, Y. Enhanced mechanical properties of ultrahigh strength Mn-Si-Cr-C steels treated by a novel bainitic transformation plus quenching and partitioning process. *Heat Treat. Surf. Eng.* **2019**, *1*, 63–71. [CrossRef]
42. Carvalho, F.M.; Centeno, D.; Tressia, G.; Avila, J.A.; Cezario, F.E.M.; Márquez-Rossy, A.; Ariza, E.A.; Masouni, M. Development of a complex microstructure on commercial carbon-silicon grade steel by governing the phase transformation mechanisms to design novel quenching and partitioning processing. *J. Mater. Res. Technol.* **2022**, *18*, 4590–4603. [CrossRef]
43. Mesplont, C. Phase Transformations and Microstructure-Mechanical Properties Relations in Complex Phase High Strength Steels. Ph.D. Thesis, Universitaire de Lille, Lille, France, 2002.
44. Stratmann, M.; Müller, J. The mechanism of the oxygen reduction on rust-covered metal substrates. *Corr. Sci.* **1994**, *36*, 327–359. [CrossRef]
45. Mehner, T.; Morgenstern, R.; Frint, P.; Scharf, I.; Wagner, M.F.X. Corrosion characteristics of a quenching and partitioning steel determined by electrochemical impedance spectroscopy. *IOP Conf. Ser.: Mater. Sci. Eng.* **2018**, *373*, 012003. [CrossRef]
46. Yang, L. *Techniques for Corrosion Monitoring*, 2nd ed.; Elservier: Cambridge, MA, USA, 2021.
47. Cetin, M. Effect of boron added corrosion behavior of cast 304 stainless steel. *Prot. Met. Phys. Chem.* **2019**, *55*, 1217–1225.